

U-Pb (LA-ICP-MS) of detrital zircon and whole rock Nd and geochemical constraints on the provenance, depositional age and tectonic setting of the metasedimentary Piriá Basin, northern Brazil: implications for the evolution of the Gurupi Belt

U-Pb (LA-ICP-MS) em zircão detrítico e dados geoquímicos e de Nd em rocha total como parâmetros controladores da proveniência, idade deposicional e ambiente tectônico da Bacia metassedimentar do Piriá, norte do Brasil: implicações para evolução do Cinturão Gurupi

Elem Cristina dos Santos Lopes^{1*}, Evandro Luiz Klein^{2,3}, Candido Augusto Veloso Moura³, Fernando Rodrigo dos Anjos Lucas³, Bruno Luiz Silva Pinheiro³, Joseneusa Brilhante Rodrigues¹, Margarete Wagner Simas¹

ABSTRACT: The Piriá Basin (Piriá Formation) is a hemi-graben shaped basin that developed over Precambrian rocks of the Gurupi Belt. The lithological content comprises four interfingering lithofacies: (1) arkose and greywacke with pelite layers, (2) laminated siltstones and pelites, (3) arkose with hummocky stratification, and (4) oligomitic conglomerate. This sequence was formed in alluvial fans (conglomerate), and fluvial systems (arkose, greywacke, siltstones and pelites) that were established and evolved during the migration of the subsidence. The sedimentary sequence underwent anquimetamorphism and very weak tectonic deformation. U-Pb analyses of detrital zircon set the maximum depositional age at 591 Ma and indicate several sediment sources, that range in age from the Neoproterozoic to the Archean. The main sources are from the Rhyacian, which is the main period of continental crust formation in the São Luís cratonic fragment and the basement of the Gurupi Belt. Neoproterozoic sources were important in the eastern segment of the basin. Ages from unknown sources in the region so far have also been recorded. Combined, the U-Pb zircon data, the whole-rock geochemical and Sm-Nd results, and the petrographic information revealed proximal felsic to intermediate provenance, in addition to recycled sedimentary sources. As a whole, our data suggest that the Piriá Formation was deposited in a post-orogenic basin related to the final stage of evolution of the Brasiliano cycle of orogenies, which built up the Gurupi Belt.

KEYWORDS: Brasiliano/Pan-african cycle; Provenance; Post-orogenic basins; Sedimentology; Gurupi Belt; São Luís craton.

RESUMO: A Bacia do Piriá (Formação Piriá) é um rifte com forma de hemi-graben desenvolvido sobre rochas pré-cambrianas do Cinturão Gurupi. O conteúdo litológico se distribui em quatro litofácies que ocorrem interdigitadas: (1) arcóseos e grauvacas com níveis de pelitos, (2) siltitos e pelitos laminados, (3) arcóseos com estrutura hummocky, e (4) conglomerado oligomítico. Esse conjunto se formou em leques aluviais (conglomerados) e em sistema fluvial (arcóseos, grauvacas, siltitos e pelitos) que se estabeleceu e evoluiu à medida que a subsidência avançou e sofreu anquimetamorfismo e deformação tectônica muito leve. Análises U-Pb em zircão detrítico estabelecem idade máxima para a sedimentação em 591 Ma e indicam fontes detríticas com idades muito variáveis, do Neoproterozoico ao Arqueano. As fontes principais são do período Riaciano, que representa o principal período de formação de crosta continental no Fragmento Cratônico São Luís e no embasamento do Cinturão Gurupi. Fontes importantes do Neoproterozoico foram identificadas no segmento oriental da bacia. Fontes com idades desconhecidas na região foram também identificadas. Combinados, os dados U-Pb em zircão detrítico, os dados geoquímicos e de isótopos de Sm-Nd em rocha total, e petrográficos revelam proveniência principal a partir de rochas fêlsicas e intermediárias proximais e de fontes sedimentares retrabalhadas. Em conjunto, os resultados indicam que a Formação Piriá se depositou em bacia pós-orogênica relacionada com o estágio final do ciclo orogênico Brasiliano, responsável pelo soerguimento do Cinturão Gurupi.

PALAVRAS-CHAVE: Ciclo Brasiliano/Pan-africano; Proveniência; Bacias pós-orogênicas; Sedimentologia; Cinturão Gurupi; Cráton São Luís.

¹Geological Survey of Brazil – CPRM. E-mails: elem.lobes@cprm.gov.br, joseneusa.rodrigues@cprm.gov.br, margarete.simas@cprm.gov.br

²Economic Geology Division, Geological Survey of Brazil – CPRM. E-mail: evandro.klein@cprm.gov.br

³Program of Post-Graduation on Geology and Geochemistry, Universidade Federal do Pará – UFPA. E-mails: flucas@yahoo.com.br, bruico@yahoo.com.br, candido@ufpa.br

*Corresponding author.

Manuscript ID: 20150015. Received in: 07/16/2015. Approved in: 01/05/2016.

INTRODUCTION

From the end of the Brasiliano orogenic cycle (Ediacaran-Cambrian transition), Paleozoic intracratonic basins and Mesozoic to Cenozoic sedimentary covers formed during the various stages (transition, stabilization and reactivation) of evolution of the South American Platform (Almeida *et al.* 2000). The Piriá Basin (Piriá Formation; Costa *et al.* 1977), which overlies Precambrian rocks of the Gurupi Belt and São Luís cratonic fragment in northern Brazil (Fig. 1), is likely associated with the post-orogenic and/or transition stages.

The spatial distribution of the Piriá Basin has recently been reviewed (Klein & Sousa 2012, Lopes & Klein 2014), but fundamental aspects about basin evolution remain unconstrained. These include the lithological content and sedimentary setting of deposition, the depositional age and sources of the sediments,

the influence of metamorphism and deformation, and the tectonic meaning of the basin. Because of the lack of fossil record and radiometric dating in the basin, Ediacaran to Cambrian times are in general inferred for the sedimentation (Abreu *et al.* 1980, Costa 2000, Pinheiro *et al.* 2003, Truckenbrodt *et al.* 2003, Klein *et al.* 2005). In addition, the basin is interpreted either as a post-orogenic cover (molasse?) related to the final stages of evolution of the Gurupi Belt (Abreu *et al.* 1980, Costa 2000, Klein *et al.* 2005, Pinheiro *et al.* 2003), or as a precursor rift of the Paleozoic intracratonic Parnaíba Basin (Lopes & Klein 2014).

In this work, we addressed some of the pending aspects listed above:

1. depositional age,
2. provenance,
3. sedimentary setting, and
4. tectonic setting.

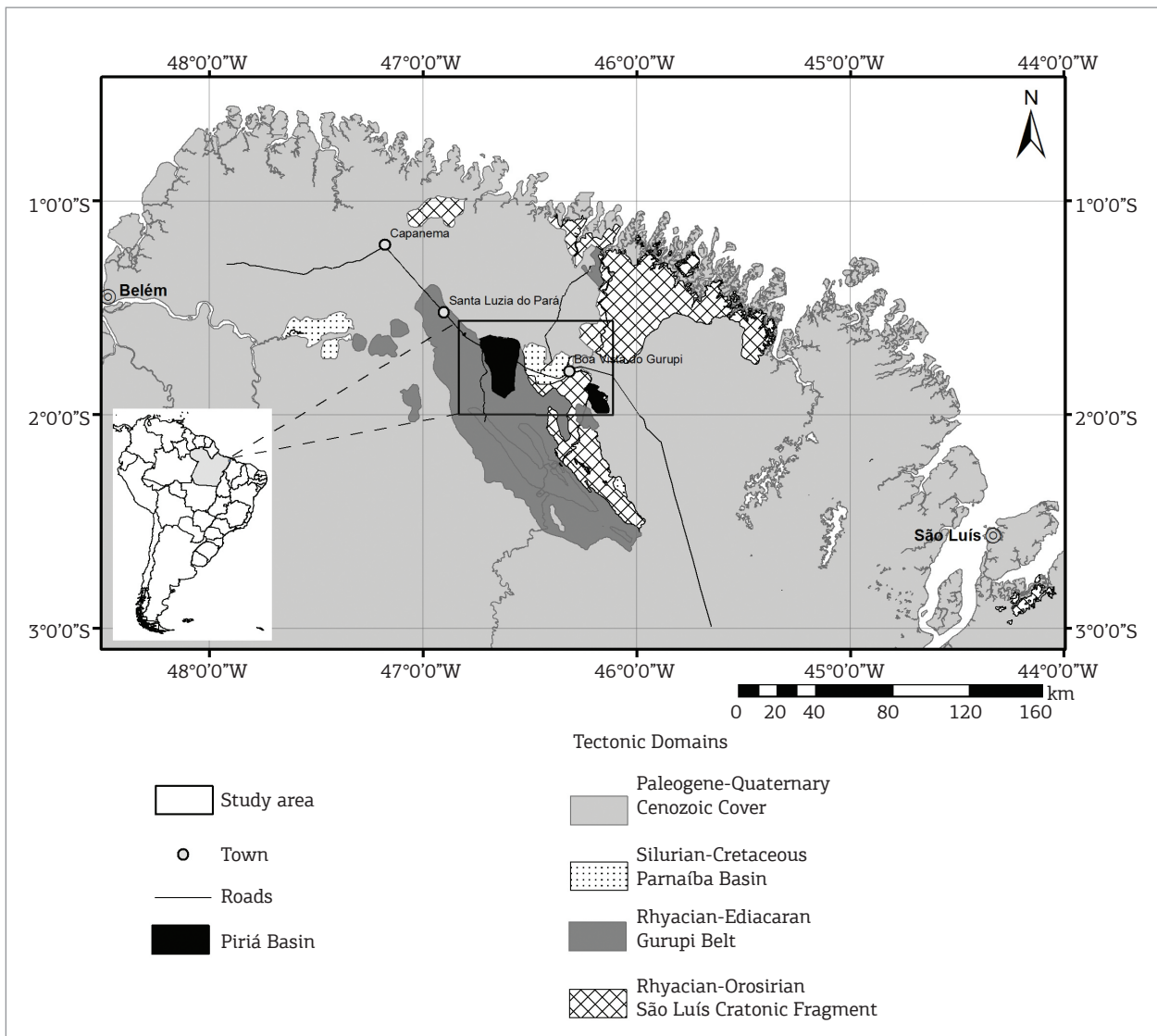


Figure 1. Location map and distribution of the Piriá Basin in relation to the tectonic domains of the study region.

This will be based on U-Pb and Pb-Pb detrital zircon ages, and whole-rock Sm-Nd and geochemical data.

GEOLOGICAL SETTING

It is beyond the scope of this paper to discuss in detail the stratigraphy of the study region. For details, the reader is referred to recent geological maps (Klein *et al.* 2008a, Klein and Lopes 2011, Klein & Sousa 2012, Lopes & Klein 2014). Only the major tectonic domains and associations are discussed here:

1. São Luís cratonic fragment,
2. Gurupi Belt, and
3. Phanerozoic sedimentary covers (Fig. 1).

The São Luís cratonic fragment comprises the metavolcano-sedimentary Aurizona Group (2240 to 2214 Ma), the juvenile, calc-alkaline granitoids of the Tromai Intrusive Suite (2168 to 2148 Ma), and the felsic to intermediate volcanic units (Rio Diamante and Serra do Jacaré formations, of 2164 to 2159 Ma) (Pastana 1995, Klein *et al.* 2008a, 2008b, 2009). All these units formed in island and magmatic arc/continental margin associations during an interpreted accretionary phase of a Rhyacian orogen. Collision-type granites are included in the Tracuateua Suite (2091 to 2086 Ma; Costa 2000, Palheta *et al.* 2009), and post-orogenic units comprise minor granites and volcanic rocks formed between 2076 and 2009 Ma (Klein *et al.* 2008b, 2009, 2014). Siliciclastic sequences (Vizeu and Igarapé de Areia formations) are younger than ca. 2078 Ma (Klein & Lopes 2011), and their tectonic setting (foreland basin?) is still uncertain.

The Gurupi Belt is interpreted as a NW-SE-trending mobile belt developed at the south-southwestern margin of the São Luís cratonic fragment during the Neoproterozoic and early Cambrian (Almeida *et al.* 1976, Klein *et al.* 2005, 2012), as part of the widespread Brasiliano orogenic cycle. The existence of tectonic activity during these era/periods is documented by a series of Rb-Sr and K-Ar ages (see primary references in Klein *et al.* 2005). The basement unit consists of an Archean metatonalite (2594 ± 3 Ma), but most of the lithological framework of the belt comprises rock units with ages that are similar to those found in the São Luís cratonic fragment, which likely represent the reworking of rocks formed in the same Rhyacian event that produced the rocks that form the present-day cratonic area. These rocks include gneisses (Itapeva Complex, 2158 to 2167 Ma), the metavolcano-sedimentary Chega Tudo Formation (2160 to 2148 Ma), a metasedimentary sequence of unknown age, and minor bodies of amphibolites (2150 ± 8 Ma) (Palheta *et al.* 2009, Klein & Lopes 2011, Klein *et al.* 2012 and references therein). A prominent feature

of the belt is the series of plutons of collision- and post-collision-type peraluminous and potassic granites to quartz-syenites formed at 2100 ± 15 Ma (Palheta *et al.* 2009, Klein *et al.* 2012). Few Neoproterozoic intrusions have been recognized to date. Notwithstanding, these intrusions are markers of different stages of evolution of the Gurupi Belt.

1. The Boca Nova Nepheline Syenite (732 ± 7 Ma, Klein *et al.* 2005) likely indicates the opening of the basin (rift) that was subsequently involved in the Neoproterozoic-Ediacaran orogeny;
2. the metamorphosed calc-alkaline Caramujinho microtonalite (624 ± 16 Ma, Klein & Lopes 2011), whose tectonic meaning is still uncertain, and
3. the collision-type Ney Peixoto granite (549 ± 4 Ma, Villas & Sousa 2007, Palheta *et al.* 2009).

The metasedimentary (passive margin?) sequences, which include the Gurupi Group and the Cabeça de Porco Formation, are interpreted as Neoproterozoic in age (Lopes & Klein 2014). The Piriá Formation, which is the subject of this paper, overlies the Gurupi Group and precedes the deposition of the Paleozoic intracratonic Parnaíba Basin.

ANALYTICAL PROCEDURES

U-Pb LA-ICP-MS analyses were undertaken at the Laboratório de Estudos Geocronológicos, Geodinâmicos e Ambientais of the Universidade de Brasília (UnB), Brasília, Brazil. The analyses followed procedures described in detail in Bühn *et al.* (2009). Concentrates of zircon were obtained by crushing the rock and then sieving and panning. Zircon crystals were hand-picked under a binocular microscope, mounted in epoxy resin, and polished with diamond paste; a conductive gold-coating was applied just prior to analysis. At UnB, the analyses were performed with a Thermo Finnigan Neptune multicollector inductively coupled plasma mass spectrometer with an attached New Wave 213 μm Nd-YAG solid state laser. The acquisition followed a standard — sample bracketing technique with four sample analyses between a blank and a GJ-1 zircon standard. The accuracy was controlled using the standard TEMORA-2 or UQZ. Raw data were reduced using an in-house program and corrections were done for background, instrumental mass-bias drift and common Pb, as described in Bühn *et al.* (2009). The ages and probability plots were calculated using ISOPLOT 3.0 (Ludwig 2003). Analyses were preceded by Cathodoluminescence and/or Backscattered Electron imagery done at UnB.

Zircon dating by the Pb evaporation method (Kober 1986) was conducted at the Laboratório de Geologia Isotópica (Pará-Isó) of the Universidade Federal do Pará, Belém, using the double

filament array. Isotopic ratios were measured in a FINNIGAN MAT 262 mass spectrometer, and data were acquired in the dynamic mode using the ion-counting system of the instrument. For each step of evaporation, a step age is calculated from the average of the $^{207}\text{Pb}/^{206}\text{Pb}$ ratios. When different steps yield similar ages, all are included in the calculation of the crystal age. Common Pb corrections were made according to Stacey and Kramers (1975), and only blocks with $^{206}\text{Pb}/^{204}\text{Pb}$ ratios higher than 2500 were used for age calculations. $^{207}\text{Pb}/^{206}\text{Pb}$ ratios were corrected for mass fractionation by a factor of 0.12‰ per a.m.u, given by repeated analysis of the NBS-982 standard, and analytical uncertainties are given at the 2σ level.

Whole rock Sm-Nd analyses were undertaken at the UnB and UFPA laboratories, and the analytical procedures for Sm-Nd analyses are described in Gioia and Pimentel (2000). Fifty mg of whole rock powders were mixed with a $^{149}\text{Sm}/^{150}\text{Nd}$ spike and dissolved in Savilex vessels. The Sm-Nd separation used cation exchange Teflon columns with Ln-Spec resin, then Sm and Nd were deposited in Re filaments, and the isotopic ratios were determined on a FINNIGAN MAT 262 mass spectrometer using the static mode. The Nd data were normalized to a $^{146}\text{Nd}/^{144}\text{Nd}$ ratio of 0.7219 and uncertainties in the Sm/Nd and $^{143}\text{Nd}/^{144}\text{Nd}$ ratios were about 0.4% (1σ) and 0.005% (1σ), respectively, based on repeated analysis of the BHVO-1 and BCR-1 standards. The crustal residence ages were calculated using the values of DePaolo (1981) for the depleted mantle (T_{DM}).

Whole rock powders were analyzed at the Acme Analytical Laboratories Ltd. in Vancouver, Canada, by Inductively Coupled Plasma Emission Spectrometry (ICP-ES) for major elements and Inductively Coupled Plasma Mass Spectrometry (ICP-MS) for trace elements, including the rare-earth elements, after fusion with lithium metaborate/tetraborate and digestion by diluted HNO_3 . Loss on ignition (LOI) was determined by weight difference after ignition at 1,000°C. Blank analyses were always below the minimum detection limit for each element, and the analytical protocol included the analysis of the reference materials (standards) CSS, DS7, SO-18, and OREAS76A.

THE PIRIÁ BASIN

General aspects

According to Lopes and Klein (2014), the Piriá Formation crops out in three basin segments that cover older units of the Gurupi Belt and of the São Luís cratonic fragment (Fig. 1). The thickness of the basin is unknown. The main and largest basin segment forms a hemi-graben with the main axis oriented to the north-south direction. This segment is limited to the west by a grossly north-south-trending, high-angle normal fault with associated conglomerate beds. The normal fault

was displaced by orthogonal transfer faults (Figs. 2 and 3). The east-limiting normal fault is more continuous, dips with shallower angles and lack conglomerates associated to the fault plane. Limited paleocurrent information indicates preferential flow direction to the northwest and southwest. The western and smallest segment of the basin lies discordantly over the metasedimentary Cabeça de Porco Formation. The eastern segment has normal faulted contacts with granitoids of the basement, and the northern portion of this segment was displaced by post-sedimentation normal or strike-slip faults.

Lithological content

Historically, the Piriá Formation has been described as composed of arkose, subarkose, greywacke and subordinate conglomerate, siltstones with thin marble layers, and shale (Abreu *et al.* 1980, Costa 2000, Truckenbrodt *et al.* 2003). Some lines of evidence indicate that the rocks of the Piriá Formation underwent very low degree of metamorphism (anquimetamorphism), which includes (Costa 2000, Truckenbrodt *et al.* 2003, and this study):

1. the high degree of diagenesis,
2. presence of neofomed epidote in sandstones,
3. the large amount of sericite in pelites,
4. presence of local cleavage, and
5. presence of local polygonal texture.

Therefore, the prefix “meta” is implicit in the following descriptions of the Piriá rocks.

In this work, we suggest that the formation is composed of four sedimentary lithofacies (Fig 3):

1. arkose and greywacke with pelite layers,
2. laminated siltstone and pelite,
3. arkose with hummocky stratification, and
4. oligomictic conglomerate.

Only the conglomerate facies has been separated in the geological map by Lopes and Klein (2014). Syn-rift basal units, which are commonly observed in similar basins elsewhere, have not been observed in the Piriá Basin. These include siliciclastic sequences formed in response to early fault displacements, in subaerial settings, with water supply enough to sustain fluvial systems (e.g., Prosser 1993).

Lithofacies ap: arkose and greywacke with pelite layers

This facies can be observed in the northeastern portion of the main segment of the Piriá Basin (Fig. 3), and occurs in gradational contact with the laminated siltstones and pelites (Sp lithofacies). The arkoses are greenish grey, medium- to fine-grained and moderately sorted rocks, with plane-parallel lamination (Fig. 4A). They are composed of

quartz (60%), feldspars (35%, predominantly plagioclase) and minor amounts of opaque minerals, zircon, garnet, epidote, sericite, biotite, chlorite and tourmaline. Epidote comprises detrital grains and grains formed from alteration of plagioclase, indicating anquimetamorphism (Fig. 4B). The dissemination of chlorite gives the greenish color to the rocks. Some portions of this facies have more than 15%

greenish, slightly oriented matrix composed of quartz and chlorite and represent greywackes. These are well-sorted, fine- to very fine-grained rocks with sub-angular grains of quartz (30%), feldspars (40%) and lithic fragments (<11%). Detrital and neoformed epidote is common. The shales are brownish and greenish, fine-grained and laminated rocks, which are unevenly crosscut by thin quartz veinlets. Dykes of

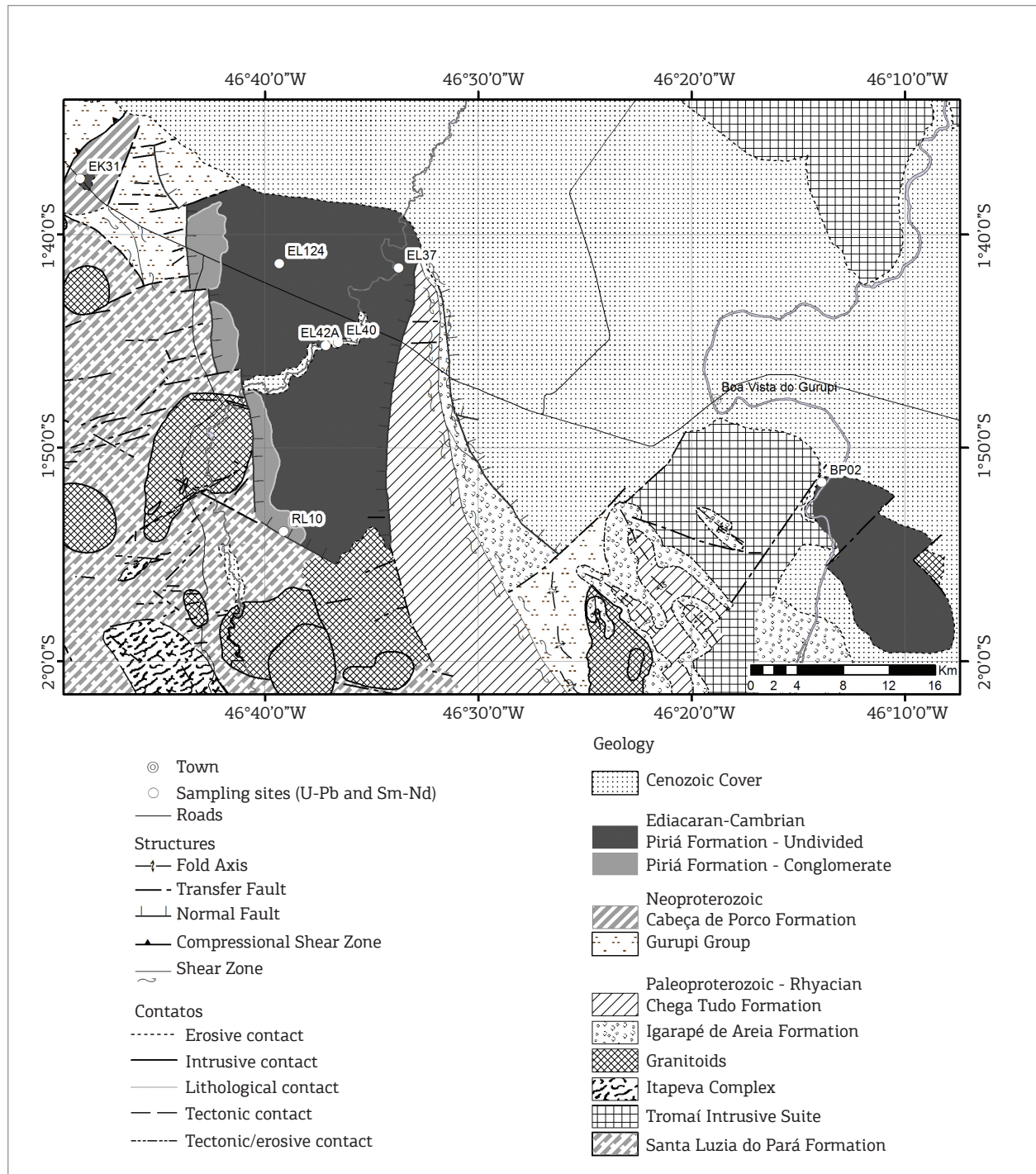


Figure 2. Simplified geological map of the study area (adapted from Lopes & Klein 2014 and Klein & Sousa 2012), with location of samples used in geochronological and Nd analyses.

mafic rocks and carbonate-quartz-epidote small veinlets are locally observed, indicating possibly hydrothermal alteration.

Lithofacies sp: laminated siltstones and pelites

this lithofacies is observed in the central-southern portion of the main basin segment. The fine-grained rocks show greenish grey to reddish colors and plane-parallel to slightly undulated lamination, which is characterized by the alternation of silt and clay layers (Fig. 4C). Tiny sericite flakes are visible only under the microscope. Very fine grained layers of subarkose and arkose occur interstratified within the layers of siltstone and pelites. The poorly sorted arkose/subarkose is composed of subangular grains of quartz (64 to 95%), K-feldspar and plagioclase (2 to 32%), and up to 11% of lithic fragments. The matrix totalizes 10% of the rocks and comprises quartz and muscovite. Well rounded feldspar grains indicate possible reworking of the associated arkoses. The transition between siltstones/pelites and arkose/subarkose is gradational.

Lithofacies ah: arkose with hummocky stratification

This lithofacies crops out in the western and main segments of the basin. It is composed of greenish grey, fine-

medium-grained and moderately sorted arkoses. The rocks show a variety of sedimentary structures, including plane-parallel stratification with tangential lamination at the top and base of the foresets, stratification truncated by wave-ripples, hummocky cross-stratification (Fig. 4D), large-scale cross-bedding, and local convolute structures (Fig. 4E), which are typical of subaqueous environment. Thickening of the arkose layers toward the top of the sedimentary package is observed locally. Coarse-grained and micro-conglomeratic sandstones are also common. The sandstones are well-sorted rocks composed of subrounded to angular grains of quartz (92%), feldspars (5%), and lithic fragments. Well-preserved detrital grains of epidote are commonly observed, indicating proximal source areas.

Lithofacies cg: oligomictic conglomerate

this lithofacies crops out along the fault that limits the western margin of the main basin segment (Figs. 2 and 3). The conglomerates are predominantly matrix-supported rocks, with clasts of quartz and rarely of metamorphic rocks. The quartz clasts are 1 to 3 cm large, subangular and set in a matrix composed predominantly of quartz and muscovite, and minor biotite and fine-grained rock fragments

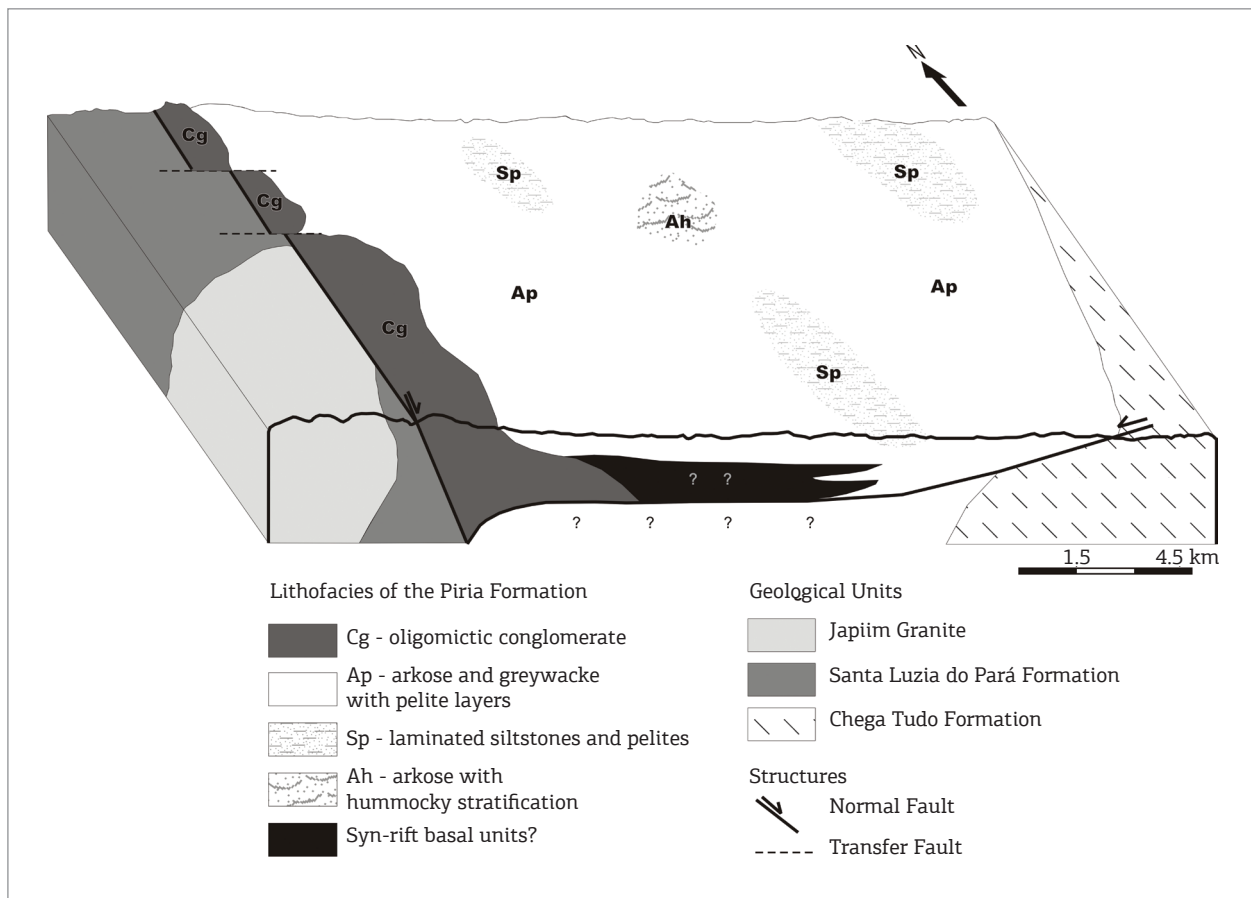


Figure 3. Schematic block diagram depicting the spatial relationships of the Piriá Basin, structural features and lithofacies subdivision.

(Fig. 4F). Grains of muscovite are usually larger than those of other matrix minerals. Layers composed of mottled silt and clays occur as intercalations in the conglomerate package and show sharp, rarely gradational contacts. X-rays analysis detected the presence of abundant smectite and subordinate kaolinite, quartz and mica.

GEOCHEMISTRY

Major and trace elements

Whole rock major and trace elements results are presented in Table 1. The samples show large variability in

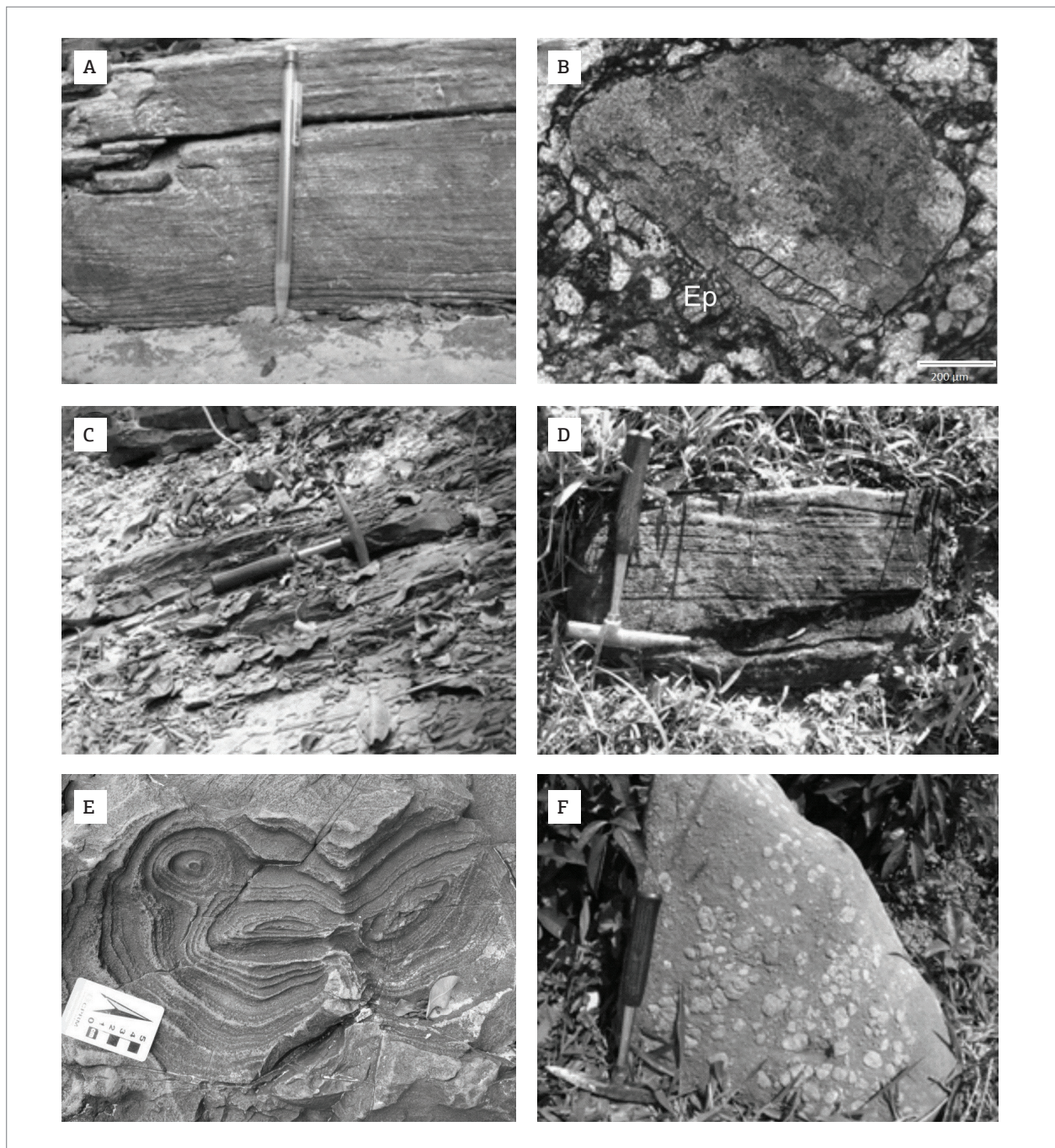


Figure 4. Field and microscopic aspects of rocks of the Piriá Formation. (A) Arkose of the Ap lithofacies with plane-parallel lamination. (B) Photomicrograph (crossed polarizers) of the arkose showing epidote crystals around detrital quartz. (C) Laminated siltstone of the Sp lithofacies. (D) Arkose of the Ah lithofacies with hummocky stratification. (E) Convolute structures in arkose. (F) Conglomerate with quartz pebbles.

Table 1. Major and trace elements chemical composition of samples from the Piriá Formation.

Sample	EK31	EL42A	EL43	EL54	EL128	EL165A	EL40	EL44A	EL124	EL34	BP02
Chemical classification	Subarkose	Arkose	Litharenite	Litharenite	Litharenite	Litharenite	Litharenite	Greywacke	Greywacke	Greywacke	Fe-Sand
SiO ₂ (wt.%)	90.94	82.74	81.06	77.23	76.31	75.43	73.71	72.59	69.75	67.91	70.87
Al ₂ O ₃	4.80	8.85	9.36	10.48	9.65	11.42	9.45	12.46	13.85	15.26	12.59
Fe ₂ O ₃	0.36	1.51	2.03	3.26	4.37	3.05	5.39	4.12	4.03	3.87	6.03
MgO	0.09	0.37	0.65	1.10	0.80	1.07	0.87	1.01	1.56	1.61	1.59
CaO	0.09	0.12	0.41	0.64	1.31	1.19	1.79	0.94	1.68	2.02	1.46
Na ₂ O	1.30	2.17	3.25	3.23	2.45	3.38	2.50	3.52	4.71	4.47	4.10
K ₂ O	1.23	1.65	1.23	1.59	1.69	1.85	1.50	1.40	1.57	1.85	1.42
TiO ₂	0.06	0.44	0.29	0.54	0.68	0.56	0.73	0.58	0.65	0.41	0.72
P ₂ O ₅	0.03	0.05	0.09	0.09	0.13	0.14	0.10	0.17	0.18	0.12	0.13
MnO	0.01	0.01	0.03	0.04	0.06	0.05	0.07	0.04	0.06	0.06	0.11
Cr ₂ O ₃	<0.002	0.007	0.003	0.009	0.006	0.011	<0.01	0.009	0.010	0.011	0.010
LOI	1.10	1.90	1.50	1.60	2.40	1.70	1.93	3.00	1.80	2.30	2.80
Sum	100.00	99.84	99.92	99.82	99.82	99.83	98.03	99.84	99.83	99.86	99.92
C-Total	<0.02	0.05	0.04	0.04	0.21	0.04	0.35	0.39	0.03	0.15	0.03
S-Total	0.05	0.02	0.17	0.02	0.07	0.06	0.02	0.05	0.07	0.04	<0.01
Pb(ppm)	3.9	3.6	7.6	1.5	3.3	6.3	8.8	12.9	9.3	2.2	nd
Ni	3.4	5.6	18.4	14.9	23.9	15.2	19.0	34.3	24.4	17.8	nd
Ba	310.0	711.0	453.0	532.0	432.0	516.0	379.0	661.0	563.0	578.0	nd
Co	0.6	2.6	7.3	8.0	8.5	6.7	6.9	12.4	12.2	12.4	nd
Cs	0.6	0.8	0.4	0.6	1.7	0.9	1.5	1.0	0.5	2.3	nd
Ga	3.8	8.8	9.3	11.9	11.1	11.7	9.4	12.5	14.0	17.2	nd
Hf	1.2	11.0	3.6	11.4	9.3	11.0	7.3	8.3	6.9	4.2	nd
Nb	1.5	7.6	4.0	8.7	9.0	9.0	6.9	8.7	8.7	4.3	nd
Rb	34.1	47.0	29.2	39.6	50.3	50.0	37.1	39.4	33.7	55.3	nd
Sc	1.0	6.0	5.0	9.0	8.0	8.0	4.2	9.0	11.0	9.0	11.0
Sr	86.5	190.9	196.3	233.1	182.3	219.2	166.6	266.6	302.5	411.7	nd
Ta	<0.1	0.5	0.2	0.6	0.7	0.5	0.6	0.4	0.5	0.2	nd
Th	1.1	6.1	3.8	6.0	6.7	5.4	4.5	5.8	5.3	4.0	5
U	<0.1	1.5	1.0	1.6	1.7	1.4	1.2	1.3	1.2	0.6	nd
V	16.0	43.0	39.0	67.0	64.0	63.0	<1	65.0	86.0	62.0	nd
Zr	42.9	424.0	111.1	471.1	370.1	407.8	335.9	291.0	238.7	146.9	276
Y	23.4	28.2	9.1	19.2	27.7	21.4	20.6	20.4	25.8	11.8	20
La (ppm)	22.70	26.10	6.90	19.30	27.20	27.10	29.90	28.00	34.50	19.30	26.30
Ce	69.30	53.10	15.30	40.30	62.90	54.10	61.60	54.80	69.10	38.60	59.10
Pr	9.86	6.30	2.11	5.34	7.75	5.85	6.72	5.78	7.33	4.29	7.36
Nd	51.90	24.90	8.00	22.00	30.80	28.80	26.80	28.20	34.10	20.80	28.50
Sm	10.50	4.57	1.78	4.35	5.62	5.06	5.50	4.96	5.96	3.57	5.30
Eu	2.53	1.14	0.50	1.14	1.42	1.27	1.41	1.26	1.52	1.01	1.23

Continue...

Table 1. Continuation.

Sample	EK31	EL42A	EL43	EL54	EL128	EL165A	EL40	EL44A	EL124	EL34	BP02
Chemical classification	Subarkose	Arkose	Litharenite	Litharenite	Litharenite	Litharenite	Litharenite	Greywacke	Greywacke	Greywacke	Fe-Sand
Gd	7.68	4.86	1.57	3.88	5.21	4.67	5.71	4.47	5.35	3.04	4.38
Tb	1.00	0.78	0.28	0.64	0.85	0.60	0.84	0.58	0.72	0.35	0.79
Dy	5.98	4.25	1.62	3.50	4.73	3.89	4.31	3.93	4.94	2.36	3.95
Ho	0.97	0.89	0.33	0.70	0.89	0.78	0.84	0.78	0.97	0.45	0.77
Er	2.36	2.26	1.00	1.97	2.72	2.26	2.45	2.19	2.79	1.22	2.41
Tm	0.34	0.37	0.16	0.33	0.40	0.34	0.39	0.34	0.44	0.20	0.34
Yb	1.92	2.18	1.02	2.02	2.51	2.14	2.40	2.11	2.78	1.27	2.07
Lu	0.23	0.33	0.15	0.32	0.41	0.33	0.39	0.32	0.40	0.19	0.33
Eu/Eu*	0.86	0.74	0.91	0.85	0.80	0.80	0.62	0.82	0.82	0.94	0.76
LaN/YbN	7.97	8.07	4.56	6.44	7.31	8.54	33.00	8.95	8.37	10.25	8.44
LaN/SmN	1.36	3.59	2.44	2.79	3.04	3.37	<0.1	3.55	3.64	3.40	3.12
CeN/YbN	3.75	1.49	1.39	1.60	1.61	1.69	8.00	1.70	1.55	2.26	7.28
CeN/SmN	9.34	6.30	3.88	5.16	6.48	6.54	<0.1	6.72	6.43	7.86	2.69
EuN/YbN	1.59	2.80	2.07	2.24	2.70	2.58	<0.02	2.67	2.80	2.61	1.62

nd: not determined

the major element chemical composition and comprise predominantly litharenite and greywacke, and subordinately arkose, subarkose and Fe-sand (Fig. 5). No geographic distribution pattern is observed in this variation. Al_2O_3 shows negative correlation ($r < -0.9$) with SiO_2 , indicating that most of the silica is present as quartz. The strong ($r > 0.9$) to moderate ($r = 0.63$ to 0.75) positive correlation with MgO and Na_2O , and with Fe_2O_3 and CaO , respectively, might be explained by the Piriá sediments being controlled by the abundance of Fe-Mg oxides/silicates, feldspars and clays, with progressive dilution by increasing quartz contents.

The rare earth elements (REE) are enriched with respect to the chondrite, and most of the samples show distribution similar to that of the upper continental crust (UCC), which is characterized by fractionation between light and heavy elements, and a weakly negative Eu anomaly (Fig. 6A). The large ion lithophile (LIL) and high field strength (HFS) elements (including some REE) are variably enriched when compared to primitive mantle values and also follow (especially the HFSE) the composition of the upper continental crust (Fig. 6C). This pattern is characterized by negative breaks in Nd, P and Ti, and by positive anomalies of Pb. The Piriá samples, however, show larger enrichment in Zr than that showed by the UCC. Three samples (EK31, EL34, EL43) do not follow the REE-LILE-HFSE patterns (Figs. 6B and 6D, neither the zircon and monazite accumulation trends.

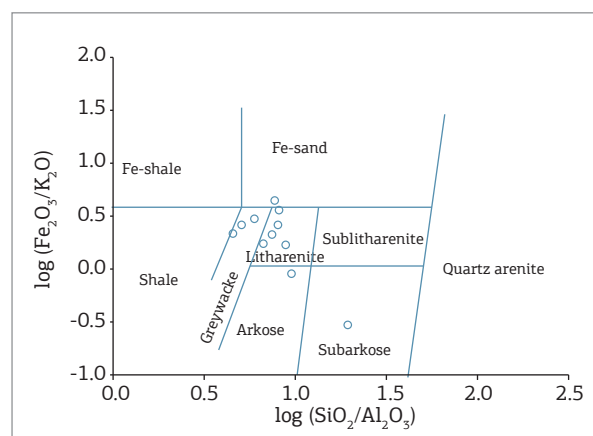


Figure 5. Chemical classification of the rocks of the Piriá Formation (Herron 1988).

Source-area weathering

The chemical index of alteration (CIA; Nesbitt & Young 1982, Nesbitt 2003) values range from 62 to 69, and plot above the feldspars join in the ACNK diagram (Fig. 7A), which indicates only moderate degree of source-area weathering. In addition, the samples plot between the granite and average shale compositions, suggesting conversion of feldspar to clays. No linear weathering trend is observed. On the other hand, the index of compositional variability (ICV; Cox *et al.* 1995, Potter *et al.* 2005) shows variance (Fig. 7B) that might be attributed

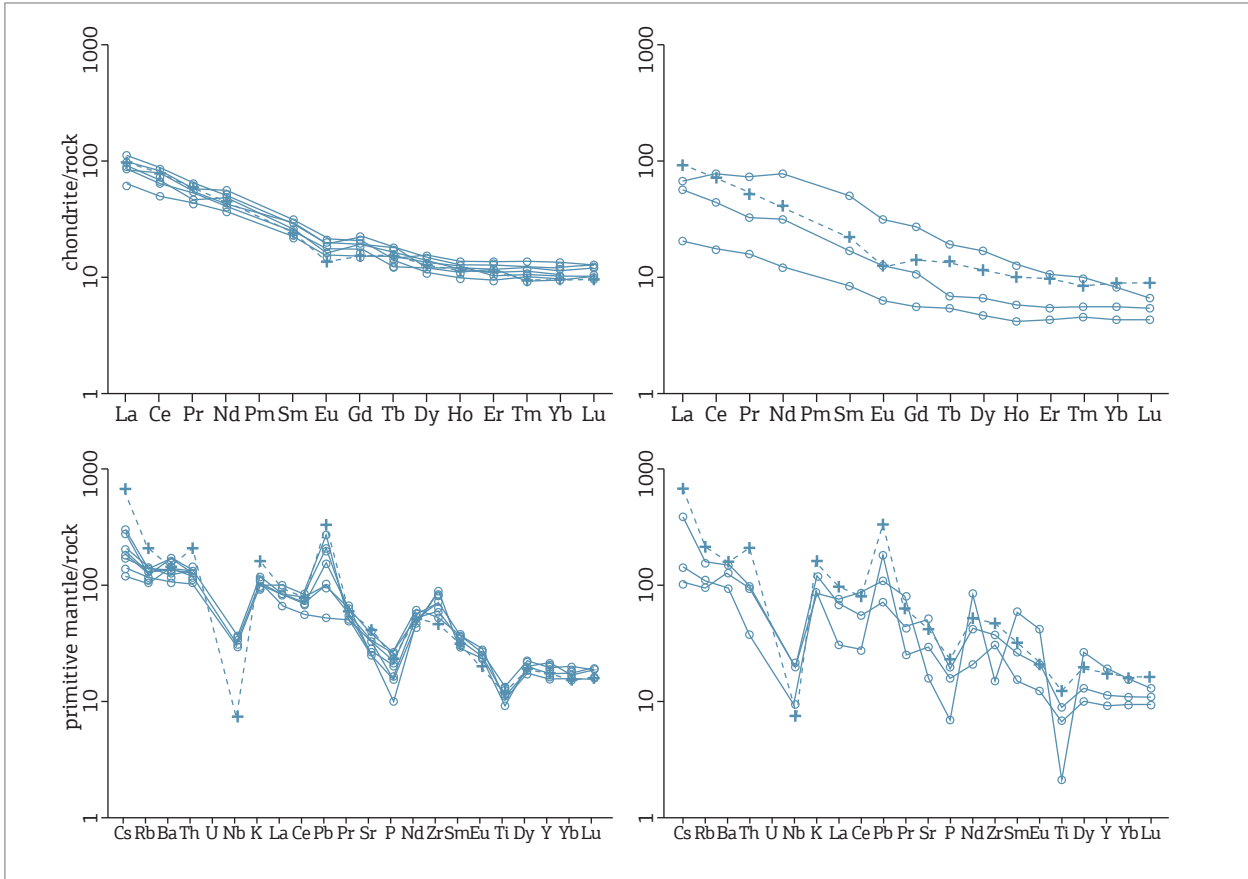


Figure 6. (A, B) Chondrite-normalized rare earth elements and (C, D) primitive mantle-normalized diagrams for the rocks of the Piriá Formation. Normalization is according to Boynton (1984) and Sun & McDonough (1989), respectively. The thick dashed line stands for the Upper Continental Crust (data from Rudnick & Gao 2005). Samples are separated into two sets for each normalization (A – C and B – D) for clarity (see text for discussion).

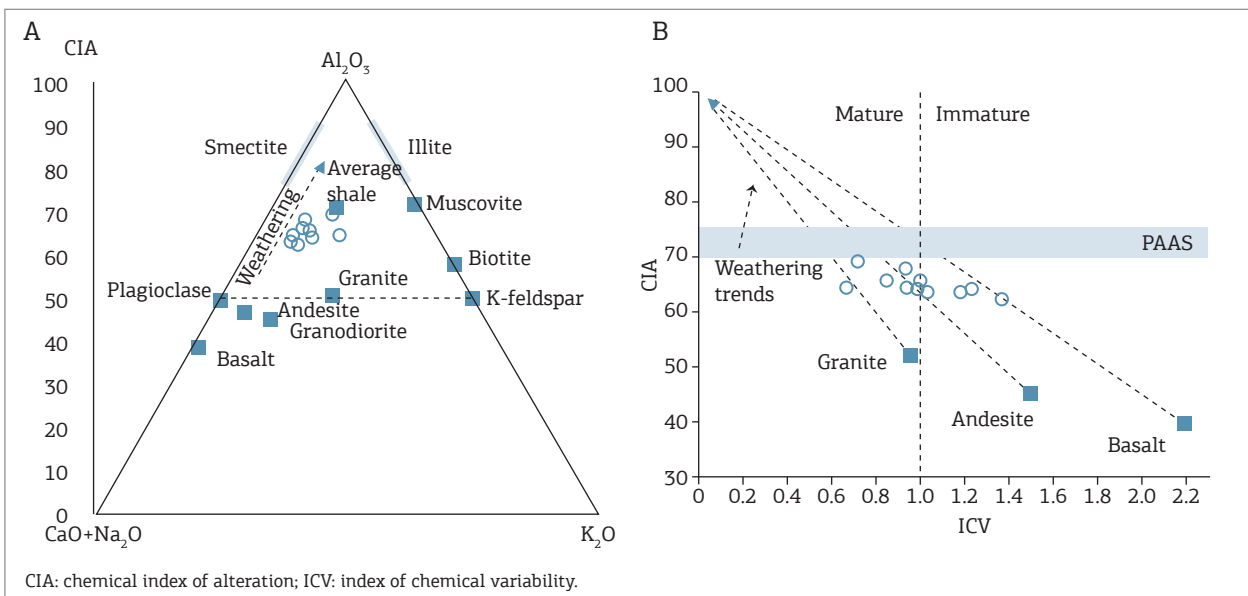


Figure 7. (A) Ternary plot of the chemical index of alteration and A-CN-K ($Al_2O_3 - CaO + Na_2O - K_2O$) diagram (Nesbitt 2003), for the sedimentary rocks of the Piriá Formation. Average rock and mineral values are from McLennan *et al.* (1993) and Pettijohn (1975). (B) Plot of chemical index of alteration versus the index of chemical variability, after Cox *et al.* (1995) and Potter *et al.* (2005). Average rock values according to LaMaskin *et al.* (2008, and references therein). PAAS is post-Archean Australian average shale (Taylor & McLennan 1985).

to differences in weathering or variation in the composition of the source rocks. Considering the large chemical variation, and the small range of CIA values, it is likely that the composition of the source rocks has played a more important role than the chemical weathering.

DETRITAL ZIRCON GEOCHRONOLOGY

U-Pb LA-ICP-MS results

Isotopic results were obtained for a greywacke (sample EL37A) from the main segment of the Piriá basin and for a subarkose (sample EK31) from the western segment. Sampling locations are shown in Figure 2, and the isotopic results of 115 zircon crystals (out of 127) that show less than 10.0% discordance and low common Pb (f^{206} below 3.0%) concentrations are presented in Table 2.

Zircon crystals from sample EL37A are nearly all euhedral to subhedral; they present inclusions, rare fractures and lack evidence of sedimentary transport. The main internal feature is the oscillatory zoning (Fig. 8A). Although rare core/rim zoning can be observed, the very low metamorphic grade of the sample and the Th/U ratios indicate that they represent events recorded in the (magmatic) source. The $^{207}\text{Pb}/^{206}\text{Pb}$ apparent ages range from 2103 ± 8 to 2234 ± 16 Ma, and all but three ages fall within the 2120 to 2180 Ma interval, forming a nearly unimodal distribution, with a peak at 2140 Ma (Fig. 9).

The crystals from sample EK31 vary widely in shape and size. Fractures and inclusions are common. Most are subrounded but of low sphericity, with oscillatory or sector zoning; some are elongated and show well-preserved prisms and pyramids, suggesting little transport, and some are fragments of larger broken crystals with oscillatory zoning (Fig. 8B). The $^{207}\text{Pb}/^{206}\text{Pb}$ apparent ages and $^{206}\text{Pb}/^{238}\text{U}$ ages (for zircons younger than 1000 Ma) spread between 563 ± 9 and 2656 ± 12 Ma, and show polymodal distribution, with three main populations peaking at 591, 2047 and 2134 Ma (Fig. 9). Several statistically subordinate populations (up to 3 crystals each) occur at 635, 935, 1100, 1290, 1530, 1960, 2045, 2204, 2356, 2450 and 2656 Ma. The youngest concordant crystal (0.8%) yielded an age of 591 ± 8 Ma.

Pb-evaporation results

The $^{207}\text{Pb}/^{206}\text{Pb}$ ages obtained by the Pb-evaporation technique must be considered only as a minimum age of the detrital zircon, given that the degree of discordance cannot be evaluated (Kober 1986). Despite this limitation, the data presented here (Table 3) showed to be useful. The two

samples comprise a conglomerate of the main segment of the basin (RL10) and the Fe-sandstone of the eastern segment (BP02).

The 12 analyzed zircon crystals from sample RL10 yielded 4 different age groups (Fig. 9). Eight crystals have ages that spread between 1514 ± 3 and 1543 ± 9 Ma, the other crystals have ages of 2064 – 2096, 2216 and 2712 Ma.

For sample BP02, only analyses undertaken at evaporation temperatures of 1,500 and 1,550°C are considered here (e.g., Kober 1986). Sixteen analyses (out of 17) yielded 4 groups of ages (Fig. 9): 526 – 566 Ma (2 crystals), 608 – 680 Ma (11 crystals), 2094 – 2105 Ma (2 crystals), and 2158 Ma (1 crystal).

Sm-Nd results

The whole rock Sm-Nd concentrations and isotopic ratios are shown in Table 4, with calculated values for the epsilon parameter and the depleted mantle model ages (T_{DM}). Samples show low REE contents, with Sm ranging from 0.63 to 6.51 ppm, and Nd between 3.23 and 29.9 ppm. The Sm/Nd ratios are mostly normal for clastic sedimentary rocks (e.g., McLennan & Hemming 1992), except for the high value (and high $^{147}\text{Sm}/^{144}\text{Nd}$ ratio) showed by sample EL42A. Model ages vary from 1.55 to 2.09 Ga (with a higher T_{DM} age of 2.42 Ga for sample EL42A), and the ϵ_{Nd} values calculated back to 540 Ma range from -5.8 to -15.4.

DISCUSSION

Depositional age

One zircon in sample BP02 (02/04) show an age of 407 ± 10 Ma, which is isolated and quite distinct from the populations age found in this sample. Since we cannot evaluate the degree of discordance of this analysis, and considering only the U-Pb results, a maximum depositional age for the Piriá Formation is indicated by the well-constrained peak at 591 Ma (Fig. 9), which is also the age of the youngest concordant zircon. This age is compatible with the geological evidence, which lead previous interpretations to establish the Ediacaran-Cambrian transition as the time of sedimentation (Abreu *et al.* 1980, Klein *et al.* 2005, Lopes & Klein 2014). The timing of rifting and the beginning of sedimentation (fault-related conglomerate deposition) remain uncertain. Considering that the collision-type Ney Peixoto Granite intruded at 549 ± 4 Ma, that the Piriá Formation presents anquimetamorphism, which is not present in the sedimentary rocks from the intracratonic Parnaíba Basin, and that no fossil record has been detected so far in the Piriá Formation, which differs from the fossil-rich Parnaíba Basin, the main

Table 2. U-Pb isotopic results from detrital zircon of the Piriá Formation.

Zircon/spot	f206(%)	Th	²⁰⁶ Pb	²⁰⁷ Pb	Error (%)	²⁰⁷ Pb	Error (%)	²⁰⁶ Pb	Error (%)	Rho	Apparentages						Conc. (%)
											²⁰⁷ Pb	(Ma)	²⁰⁷ Pb	(Ma)	²⁰⁶ Pb	(Ma)	
EK31																	
59-37	0.01	0.30	124678	0.057684	1.78	0.726	2.49	0.091344	1.74	0.69	518	39	554	11	563	9	108.83
67-43	0.04	0.43	48882	0.060212	1.50	0.781	2.29	0.094130	1.73	0.75	611	32	586	10	580	10	94.88
03-01	0.03	0.22	69433	0.059874	1.22	0.792	1.75	0.095931	1.25	0.70	599	26	592	8	591	7	98.58
93-63	0.02	0.23	78110	0.059789	1.13	0.792	1.82	0.096055	1.43	0.78	596	24	592	8	591	8	99.21
53-31	0.08	0.24	21213	0.061505	2.07	0.816	3.64	0.096179	2.99	0.82	657	44	606	16	592	17	90.11
46-26	0.03	0.15	69737	0.061333	1.20	0.833	2.13	0.098511	1.76	0.82	651	26	615	10	606	10	93.05
74-48	0.08	0.36	20296	0.061344	1.68	0.888	2.40	0.105045	1.72	0.71	651	36	646	11	644	11	98.86
80-54	0.07	0.58	26974	0.059852	3.08	0.869	4.70	0.105291	3.54	0.75	598	67	635	22	645	22	107.88
73-47	0.03	0.62	64484	0.069217	0.98	1.489	1.57	0.156024	1.22	0.77	905	20	926	10	935	11	103.25
86-58	0.05	0.20	34996	0.077212	1.15	2.013	2.50	0.189123	2.22	0.89	1127	23	1120	17	1117	23	99.11
48-28	0.01	0.01	332083	0.083884	0.41	2.670	0.97	0.230841	0.88	0.89	1290	8	1320	7	1339	11	103.80
05-03	0.01	0.09	252876	0.093433	0.37	3.171	0.66	0.246123	0.54	0.77	1497	7	1450	5	1418	7	94.77
19-15B	0.01	0.16	320724	0.095026	0.28	3.578	0.64	0.273056	0.57	0.86	1529	5	1545	5	1556	8	101.81
20-15N	0.01	0.15	185841	0.095612	0.27	3.719	0.60	0.282103	0.53	0.85	1540	5	1575	5	1602	8	104.01
10-08	0.00	0.28	1038541	0.120137	0.33	5.731	0.72	0.345961	0.64	0.86	1958	6	1936	6	1915	11	97.81
95-65	0.02	0.28	96247	0.129662	0.68	6.304	2.32	0.352622	2.22	0.95	2093	12	2019	20	1947	37	93.01
04-02	0.00	0.49	434707	0.122306	0.30	6.130	0.94	0.363493	0.89	0.94	1990	5	1994	8	1999	15	100.43
88-60	0.02	0.46	83864	0.126426	0.84	6.373	1.63	0.365582	1.39	0.85	2049	15	2029	14	2009	24	98.03
55-33	0.01	0.17	154410	0.135466	0.72	6.877	1.12	0.368174	0.85	0.74	2170	13	2096	10	2021	15	93.12
09-07	0.00	0.07	1466560	0.121464	0.31	6.195	0.63	0.369905	0.55	0.82	1978	6	2004	6	2029	10	102.58
66-42	0.01	0.09	102316	0.132569	0.64	6.907	1.24	0.377889	1.06	0.85	2132	11	2100	11	2066	19	96.91
70-46	0.01	0.43	113367	0.126330	0.78	6.641	2.08	0.381267	1.92	0.93	2048	14	2065	18	2082	34	101.69
15-11	0.00	0.17	386316	0.130787	0.34	6.911	0.76	0.383224	0.68	0.87	2109	6	2100	7	2091	12	99.18
89-61	0.02	0.10	86093	0.128293	0.85	6.797	1.82	0.384239	1.61	0.88	2075	15	2085	16	2096	29	101.03
29-22	0.01	0.14	186919	0.120560	0.36	6.391	0.65	0.384465	0.54	0.78	1965	6	2031	6	2097	10	106.75
06-04	0.00	0.28	387786	0.132846	0.23	7.053	0.52	0.385065	0.47	0.84	2136	4	2118	5	2100	8	98.31
87-59	0.02	0.27	73470	0.142845	1.08	7.643	2.51	0.388058	2.26	0.90	2262	19	2190	22	2114	41	93.45
43-24	0.06	0.22	23932	0.136810	0.86	7.336	1.22	0.388881	0.86	0.68	2187	15	2153	11	2118	16	96.82
17-13	0.01	0.28	185121	0.134946	0.37	7.275	0.62	0.390984	0.50	0.72	2163	6	2146	6	2127	9	98.34
23-16N	0.01	0.13	234749	0.132743	0.58	7.171	4.01	0.391783	3.97	0.99	2135	10	2133	35	2131	72	99.84
96-66	0.01	0.38	141027	0.127463	0.69	6.934	1.34	0.394568	1.15	0.85	2063	12	2103	12	2144	21	103.91
83-55	0.01	0.22	176548	0.132954	0.61	7.276	1.09	0.396906	0.90	0.81	2137	11	2146	10	2155	16	100.82
97-67	0.01	0.04	152675	0.127273	0.66	7.020	1.03	0.400040	0.79	0.74	2061	12	2114	9	2169	15	105.27
47-27	0.06	0.29	23472	0.133331	1.34	7.358	2.64	0.400247	2.28	0.86	2142	23	2156	24	2170	42	101.30
24-17	0.00	0.04	8117991	0.126163	0.26	6.989	0.55	0.401786	0.48	0.82	2045	5	2110	5	2177	9	106.46
50-30	0.02	0.39	63978	0.128635	0.80	7.144	1.42	0.402790	1.18	0.82	2079	14	2130	13	2182	22	104.93
45-25	0.01	0.16	208360	0.131880	0.53	7.330	1.42	0.403134	1.32	0.93	2123	9	2153	13	2183	24	102.84
60-38	0.01	0.21	251902	0.133468	0.91	7.491	1.54	0.407058	1.25	0.80	2144	16	2172	14	2201	23	102.68
79-53	0.01	0.01	227111	0.131348	0.41	7.374	0.91	0.407178	0.81	0.88	2116	7	2158	8	2202	15	104.06

Continue...

Table 2. Continuation.

Zircon/spot	f206(%)	Th	²⁰⁶ Pb	²⁰⁷ Pb	Error (%)	²⁰⁷ Pb	Error (%)	²⁰⁶ Pb	Error (%)	Rho	Apparentages						Conc. (%)						
											U	²⁰⁴ Pb	²⁰⁶ Pb	1sigma	235U	1sigma		²³⁸ U	1sigma	²⁰⁷ Pb	(Ma)	²⁰⁶ Pb	(Ma)
98-68	0.01	0.20	248927	0.125107	0.93	7.030	2.02	0.407542	1.80	0.89	2030	16	2115	18	2204	34	108.54						
84-56	0.01	0.23	230099	0.140085	0.59	7.887	1.03	0.408338	0.84	0.79	2228	10	2218	9	2207	16	99.06						
28-21	0.01	0.23	142657	0.131572	0.41	7.437	0.97	0.409966	0.88	0.90	2119	7	2165	9	2215	16	104.52						
14-10	0.00	0.24	322741	0.132608	0.36	7.498	0.71	0.410063	0.61	0.82	2133	6	2173	6	2215	11	103.86						
78-52	0.01	0.14	126840	0.135554	0.55	7.706	0.99	0.418471	0.82	0.81	2145	10	2197	9	2254	16	105.05						
49-29	0.01	0.12	120164	0.135960	0.64	7.850	1.35	0.418762	1.19	0.87	2176	11	2214	12	2255	23	103.61						
65-41	0.00	0.14	337053	0.133318	0.89	7.765	1.80	0.422452	1.56	0.87	2142	16	2204	16	2272	30	106.04						
30-23	0.00	0.20	874474	0.151360	0.61	8.925	1.84	0.427649	1.74	0.94	2361	10	2330	17	2295	33	97.19						
64-40	0.45	0.20	5998	0.150154	1.59	8.902	2.77	0.429996	2.26	0.81	2348	27	2528	25	2306	44	98.21						
07-05	0.01	0.20	163335	0.137452	0.46	8.207	1.29	0.433035	1.21	0.93	2195	8	2254	12	2319	23	105.65						
90-62	0.01	0.23	111052	0.159865	0.64	10.997	1.26	0.498927	1.09	0.85	2454	11	2523	12	2609	23	106.31						
13-09	0.00	0.15	506850	0.180334	0.69	13.173	0.92	0.529807	0.60	0.59	2656	12	2692	9	2741	13	103.19						
EL37																							
004-Z01N	0.02	0.26	97414	0.134322	0.67	7.451	1.03	0.402314	0.78	0.73	2155	12	2167	9	2180	14	101.13						
005-Z01B	0.02	0.24	70175	0.134279	0.59	7.294	0.89	0.393972	0.67	0.71	2155	10	2148	8	2141	12	99.38						
006-Z02	0.01	0.22	115389	0.134582	0.53	7.122	0.91	0.383809	0.74	0.79	2159	9	2127	8	2094	13	97.01						
007-Z03	0.01	0.19	162958	0.133629	0.41	7.142	0.77	0.387624	0.65	0.81	2146	7	2129	7	2112	12	98.40						
008-Z04	0.02	0.26	64272	0.135815	0.44	7.312	1.03	0.390483	0.93	0.89	2174	8	2150	9	2125	17	97.73						
009-Z05	0.02	0.32	92500	0.132443	0.65	7.085	1.00	0.388005	0.76	0.73	2131	11	2122	9	2114	14	99.20						
010-Z06	0.01	0.27	136576	0.134040	0.48	7.334	0.93	0.396817	0.80	0.84	2152	8	2153	8	2154	15	100.13						
014-Z08	0.01	0.35	223733	0.134480	0.45	7.281	0.96	0.392672	0.84	0.87	2157	8	2146	8	2135	15	98.98						
015-Z09	0.00	0.31	405407	0.135637	0.49	7.530	0.85	0.402660	0.70	0.79	2172	8	2177	8	2181	13	100.42						
016-Z10	0.02	0.22	91993	0.133343	0.55	7.358	1.08	0.400228	0.94	0.85	2142	10	2156	10	2170	17	101.29						
017-Z11	0.01	0.22	177187	0.133699	0.38	7.529	1.01	0.408410	0.94	0.92	2147	7	2176	9	2208	17	102.82						
018-Z12	0.01	0.22	126011	0.133025	0.38	7.526	1.13	0.410343	1.07	0.94	2138	7	2176	10	2216	20	103.66						
019-Z13	0.01	0.24	206349	0.133014	0.44	7.600	0.80	0.414383	0.67	0.80	2138	8	2185	7	2235	13	104.53						
020-Z14	0.02	0.36	95081	0.132981	0.49	7.134	1.02	0.389068	0.90	0.87	2138	8	2128	9	2119	16	99.10						
023-Z15	0.01	0.28	175757	0.132460	0.42	7.590	0.78	0.415558	0.67	0.82	2131	7	2184	7	2240	13	105.14						
024-Z16	0.00	0.11	375326	0.133982	0.31	7.713	0.66	0.417538	0.58	0.85	2151	5	2198	6	2249	11	104.58						
025-Z17	0.82	0.28	1857	0.132896	0.78	6.497	1.54	0.354583	1.33	0.87	2137	14	2046	13	1956	22	91.57						
026-Z18	0.01	0.38	137994	0.133805	0.37	7.409	0.70	0.401569	0.59	0.81	2148	6	2162	6	2176	11	101.29						
027-Z19	0.01	0.27	179955	0.132698	0.46	7.438	0.83	0.406513	0.69	0.80	2134	8	2166	7	2199	13	103.05						
029-Z21	0.03	0.28	43621	0.135926	0.46	7.378	0.90	0.393685	0.77	0.84	2176	8	2158	8	2140	14	98.34						
034-Z23	0.01	0.19	117082	0.132741	0.53	7.137	0.94	0.389968	0.78	0.80	2135	9	2129	8	2123	14	99.44						
035-Z24	0.01	0.19	184621	0.133696	0.46	7.231	0.76	0.392247	0.61	0.75	2147	8	2140	7	2133	11	99.36						
036-Z25	0.67	0.34	2259	0.134411	0.50	6.936	0.87	0.374232	0.71	0.80	2156	9	2103	8	2049	12	95.03						
039-Z28	0.01	0.23	135289	0.134064	0.58	7.621	0.91	0.412299	0.70	0.74	2152	10	2187	8	2225	13	103.42						
040-Z29	0.01	0.37	131885	0.134448	0.43	7.861	0.97	0.424035	0.87	0.88	2157	8	2215	9	2279	17	105.65						
043-Z30	0.11	0.36	14137	0.133627	0.42	7.265	0.97	0.394295	0.87	0.89	2146	7	2144	9	2143	16	99.84						

Continue...

Provenance of the Piriá Basin, Gurupi Belt

Table 2. Continuation.

Zircon/spot	f206(%)	Th	²⁰⁶ Pb	²⁰⁷ Pb	Error (%)	²⁰⁷ Pb	Error (%)	²⁰⁶ Pb	Error (%)	Rho	Apparentages						Conc. (%)								
											U	²⁰⁴ Pb	²⁰⁶ Pb	1sigma	235U	1sigma		²³⁸ U	1sigma	²⁰⁷ Pb	(Ma)	²⁰⁷ Pb	(Ma)	²⁰⁶ Pb	(Ma)
																				²⁰⁶ Pb	(Ma)	²³⁵ U		²³⁸ U	(Ma)
045-Z32	0.01	0.09	155665	0.131676	0.47	7.620	1.14	0.419707	1.03	0.90	2120	8	2187	10	2259	20	106.54								
046-Z33	0.13	0.25	11507	0.137195	1.19	7.715	1.73	0.407854	1.25	0.71	2192	21	2198	16	2205	23	100.59								
047-Z34	0.01	0.39	182689	0.133434	0.39	7.621	1.18	0.414209	1.12	0.94	2144	7	2187	11	2234	21	104.22								
048-Z35	0.02	0.26	86380	0.132725	0.78	7.090	1.29	0.387406	1.04	0.79	2134	14	2123	11	2111	19	98.90								
049-Z36	0.02	0.34	95550	0.132947	0.47	7.161	0.88	0.390630	0.74	0.82	2137	8	2132	8	2126	13	99.46								
053-Z37	0.01	0.25	110156	0.132967	0.50	7.407	1.09	0.404029	0.97	0.88	2138	9	2162	10	2188	18	102.34								
054-Z38	0.01	0.23	113865	0.132795	0.41	7.247	0.85	0.395791	0.74	0.86	2135	7	2142	8	2150	14	100.67								
055-Z39	0.02	0.27	82138	0.131710	0.62	7.666	1.31	0.422127	1.15	0.87	2121	11	2193	12	2270	22	107.04								
056-Z40	0.05	0.34	27509	0.132173	0.50	7.352	1.26	0.403437	1.16	0.91	2127	9	2155	11	2185	21	102.72								
057-Z41	0.07	0.38	21636	0.135872	0.43	6.969	0.84	0.372018	0.72	0.83	2175	7	2108	7	2039	13	93.73								
058-Z42	0.03	0.27	45930	0.135021	0.40	7.556	0.80	0.405884	0.69	0.84	2164	7	2180	7	2196	13	101.47								
060-Z44	0.03	0.29	52469	0.134307	0.40	7.508	0.78	0.405418	0.67	0.83	2155	7	2174	7	2194	13	101.81								
063-Z45	0.01	0.18	222461	0.135305	0.40	7.810	0.77	0.418614	0.66	0.82	2168	7	2209	7	2254	12	103.98								
065-Z47	0.02	0.42	68937	0.132542	0.45	7.496	1.07	0.410196	0.97	0.90	2132	8	2173	10	2216	18	103.94								
066-Z48	0.01	0.37	246809	0.133511	0.32	7.877	0.72	0.427913	0.65	0.87	2145	6	2217	7	2296	13	107.07								
067-Z49	0.01	0.19	135228	0.132440	0.50	7.377	0.83	0.404002	0.66	0.76	2131	9	2158	7	2187	12	102.67								
069-Z51	0.01	0.22	114838	0.134891	0.43	7.079	1.08	0.380599	0.99	0.91	2163	7	2121	10	2079	18	96.14								
070-Z52	0.03	0.18	49340	0.140515	0.92	7.844	1.39	0.404850	1.04	0.73	2234	16	2213	12	2191	19	98.11								
073-Z53	0.02	0.27	65324	0.136208	1.13	7.628	1.85	0.406161	1.47	0.79	2180	20	2188	17	2197	27	100.82								
074-Z54	0.97	0.48	1560	0.134972	0.57	6.816	1.46	0.366276	1.35	0.93	2164	10	2088	13	2012	23	92.98								
075-Z55	0.01	0.28	124586	0.132932	0.46	7.522	0.85	0.410389	0.71	0.81	2137	8	2176	8	2217	13	103.73								
076-Z56	0.30	0.38	4843	0.133017	0.44	7.846	0.93	0.427794	0.83	0.87	2138	8	2213	8	2296	16	107.37								
077-Z57	0.01	0.36	126619	0.133206	0.67	7.505	1.06	0.408615	0.82	0.75	2141	12	2174	9	2209	15	103.17								
079-Z59	0.01	0.16	98937	0.132652	0.37	7.460	0.76	0.407854	0.67	0.85	2133	6	2168	7	2205	12	103.36								
080-Z60	0.80	0.39	1867	0.132700	0.77	6.961	0.99	0.380426	0.61	0.58	2134	13	2106	9	2078	11	97.39								
083-Z61	0.36	0.31	4196	0.130376	0.46	6.767	0.92	0.376432	0.80	0.86	2103	8	2081	8	2060	14	97.93								
084-Z62	0.01	0.32	282019	0.132574	0.38	7.077	0.76	0.387160	0.66	0.84	2132	7	2121	7	2110	12	98.94								
085-Z63	0.00	0.26	444983	0.132864	0.34	7.547	0.86	0.411989	0.79	0.90	2136	6	2179	8	2224	15	104.11								
086-Z64N	0.00	0.17	429105	0.133356	0.33	7.179	0.73	0.390419	0.65	0.87	2143	6	2134	6	2125	12	99.17								
087-Z64B	0.01	0.13	134376	0.135889	0.72	6.782	1.68	0.361946	1.52	0.90	2175	12	2083	15	1991	26	91.54								
088-Z65	0.02	0.30	82171	0.134834	0.46	7.331	1.04	0.394341	0.93	0.88	2162	8	2153	9	2143	17	99.12								
090-Z67	0.01	0.41	247181	0.133910	0.34	7.200	0.96	0.389964	0.90	0.93	2150	6	2137	9	2123	16	98.73								
093-Z68	0.01	0.33	123213	0.134801	0.48	7.662	1.04	0.412257	0.92	0.88	2161	8	2192	9	2225	17	102.95								
094-Z69	0.00	0.30	327605	0.134569	0.36	7.594	0.86	0.409302	0.78	0.90	2158	6	2184	8	2212	15	102.47								
095-Z70	0.03	0.23	53397	0.135166	0.90	7.695	1.25	0.412900	0.86	0.66	2166	16	2196	11	2228	16	102.86								
097-Z72	0.10	0.26	14577	0.133590	0.29	7.086	0.93	0.384678	0.88	0.94	2146	5	2122	8	2098	16	97.78								
098-Z73	0.01	0.15	200913	0.137374	0.38	7.808	0.74	0.412219	0.64	0.83	2194	7	2209	7	2225	12	101.40								
099-Z74	0.01	0.22	248124	0.135047	0.35	7.042	0.68	0.378176	0.58	0.82	2165	6	2117	6	2068	10	95.53								

stage of sedimentation in the Piriá Basin took place probably in the Cambrian period.

Sedimentary setting

Airborne magnetic geophysical data and field evidence (Lopes & Klein 2014) strongly indicate that the Piriá Basin (at least its better characterized central segment) corresponds to a hemi-graben type rift, which is bounded by normal faults. Considering the depositional age, this rift was formed by

extensional tectonics that followed the end of the Brasiliano orogeny that built up the Gurupi Belt. The presence of the conglomerate facies associated with the western normal fault (Fig. 2) suggests deposition in alluvial fans, with debris flows associated with the high relief imparted by the bounding fault slope. All the other facies are likely related to the flexural portion of the basin. Accordingly, the syn-rift basal units were deposited by fluvial systems near the conglomerate unit, and with continued subsidence, this fluvial system

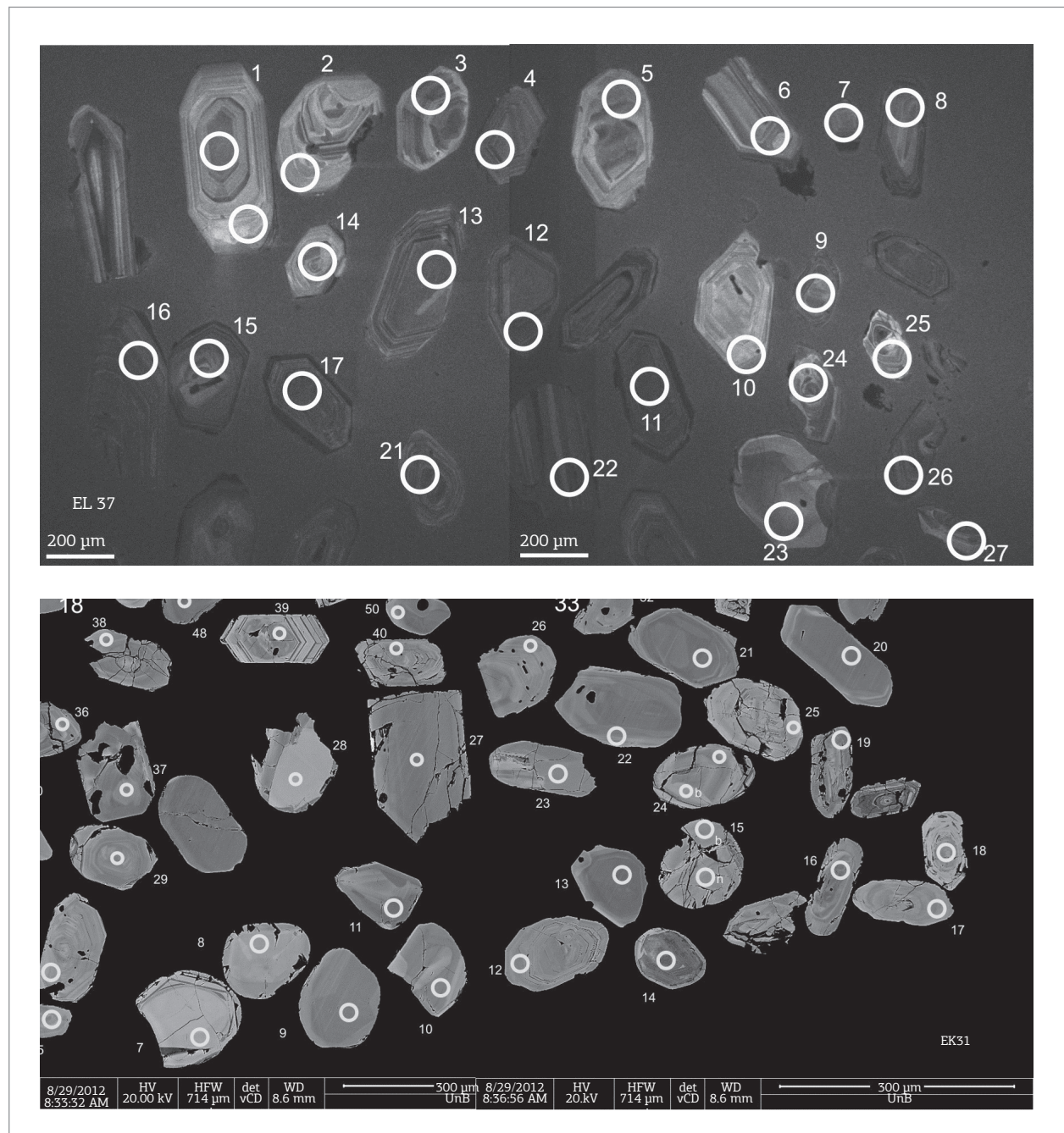


Figure 8. Cathodoluminescence (EL37) and backscattering electron (EK31) images of typical detrital zircon crystals from the Piriá Formation. Scale bars are 300 µm in A, and 200 µm in B, and the spots are numbered as in Table 2.

migrated to the central portion of the rift. The evolution of this fluvial system took place in arid/semi-arid conditions, free of chemical weathering, which permitted the preservation of feldspars and detrital epidote.

Truckenbrodt *et al.* (2003) suggested lacustrine or shallow marine setting for the deposition of the Piriá Formation. However, we understand that the presence of isolated structures that indicate storm deposited sediments (hummocky cross-stratification) is equivocal with respect to the definition of transitional to coastal sedimentary setting, and may only represent periods of instability of the subaqueous environment, such as flow variations within the fluvial canal. As such, we interpret the arkosic lithofacies (Ap and Ah) to be related to the fluvial canals, whilst the siltstone lithofacies is associated with low energy flow portions of the flood plains of the fluvial system.

Provenance

In a previous work, based on the heavy minerals content of sandstones of the Piriá Basin, mainly kyanite, staurolite, amphibole, epidote, Truckenbrodt *et al.* (2003) have suggested that proximal medium grade metamorphic rocks were the main detrital sources. These correspond to the Santa Luzia do Pará Formation and Gurupi Group, according to the present day knowledge (Lopes & Klein 2014). This is partially valid, but the abundance of plagioclase-rich arkose and greywacke indicates felsic and intermediate rocks as major sources.

Immobile/less mobile elements and their elemental ratios are useful indicators of potential source of sediments (felsic, mafic, sedimentary), and of sedimentary recycling

or hydraulic sorting. According to Fralick *et al.* (2009), in bivariate plots of immobile elements (e.g., Zr-Nb), samples that come from similar sources should align along a straight line that passes through the origin. This is not the case of the sediments of the Piriá Formation (Fig. 10A), indicating multiple sources. In addition, the Th-Ce and Ti-V relationships (Figs. 10B and 10C) indicate sources with components enriched in Th and Ti and/or hydraulic enrichment in heavy minerals that contain these elements, such as monazite and Fe-Ti oxides (magnetite, titanite), respectively. Furthermore, hydraulic sorting is also suggested by the high Zr/Sc ratios when compared to the Th/Sc ratio (Fig. 11), indicating zircon addition (McLennan *et al.* 1993), which is consistent with the high whole-rock Zr concentration (Table 1). Figure 11 also shows that most samples of the Piriá Formation plot on the compositional field of potential Rhyacian source rocks occurring in the São Luís cratonic fragment and Gurupi Belt. In the same line, several other elements and elemental ratios indicate predominance of evolved felsic to intermediate igneous and recycled sedimentary sources for the sediments of the Piriá Formation (Fig. 12).

The cumulative age probability distribution diagrams (Fig. 9) show that the main zircon sources are Rhyacian rocks (or they reworked and erosional products) with ages similar to those found in orogenic rock associations of the São Luís cratonic fragment (2240 – 2009 Ma; Klein *et al.* 2008b). The Sm-Nd data (Fig. 13) additionally support this interpretation. This is not surprising, since most of the units that crop out in the study region are Rhyacian in age.

Two other important sources have age peaks at 605 and 1517 Ma (Fig. 9). The age range of the youngest source (590 – 645 Ma) falls within the known interval of development of the Gurupi Belt (732 – 549 Ma). This range of ages also suggests that more orogenic felsic rocks might be present in the region than it is known to date, or, alternatively, that the sources might be located in adjacent Neoproterozoic orogens, such as the western portion of the Borborema Province (e.g., Ganade de Araújo *et al.* 2012). The source units for zircons with ages around 1500 Ma, which have been recorded in the conglomerate and subarkose samples, are more enigmatic. Rocks with this age are not known in the study region and are very rare in the Borborema Province (see Ganade de Araújo *et al.* 2012, Amaral *et al.* 2015). Furthermore, detrital zircons of this age in Cretaceous sediments and modern river sands from Gurupi-São Luís and Borborema are also very rare (Knudsen *et al.* 2015). These ages might represent unknown cryptic Mesoproterozoic rocks in the study area, or reworking of older sedimentary sources and distant provenance. In this regard, although these ages have been reported for sedimentary rocks of the Volta Basin in the West African Craton

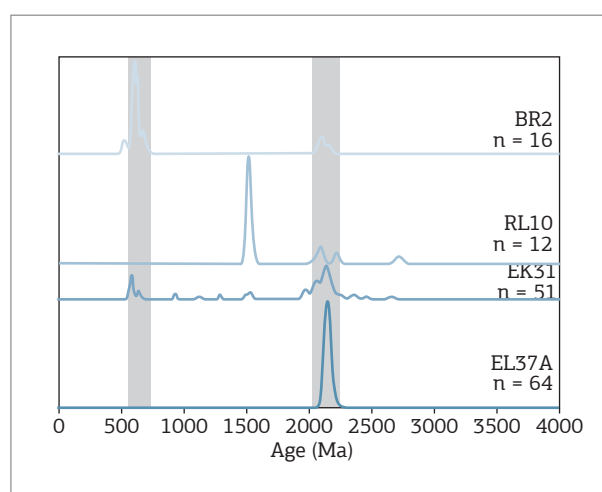


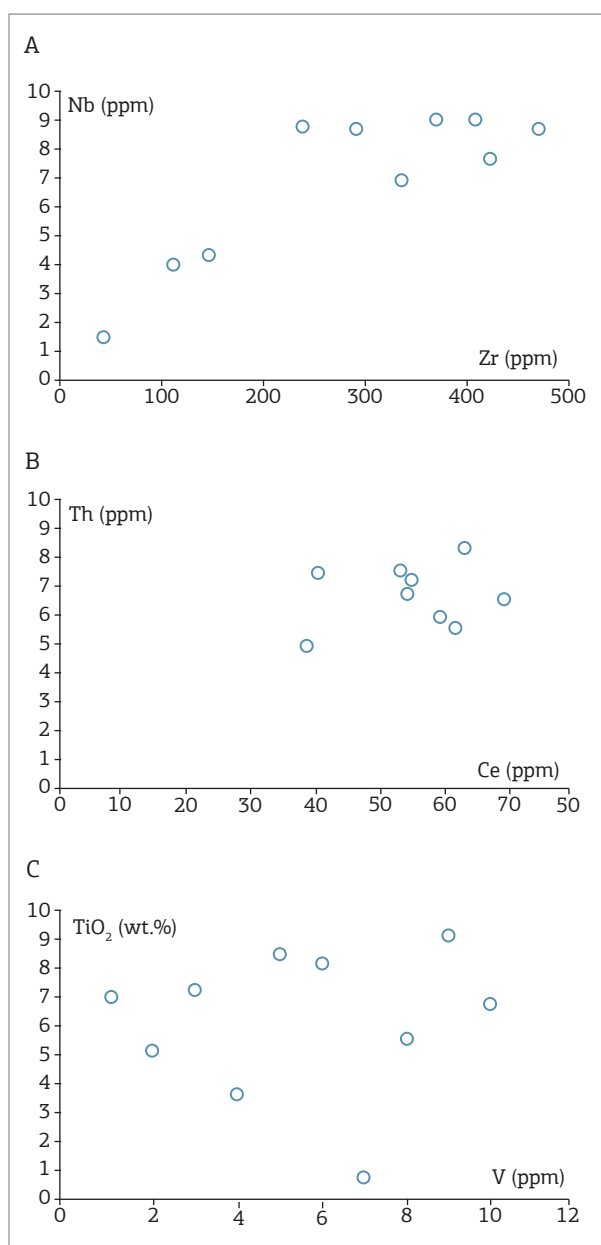
Figure 9. Cumulative age probability plots for detrital zircon of the Piriá Formation. The grey bars show the time interval of known magmatic activity in the São Luís cratonic fragment (2240 – 2009 Ma) and Gurupi Belt (732 – 549 Ma).

Table 3. Isotopic results obtained from the Pb-evaporation technique in detrital zircon from the Piriá Formation.

Zircon	T (°C)*	N° of ratios	²⁰⁴ Pb/ ²⁰⁶ Pb	²⁰⁷ Pb/ ²⁰⁶ Pb	2σ	⁽²⁰⁷ Pb/ ²⁰⁶ Pb) _c	2σ	Age (Ma)	2σ
Sample	BPO2								
02/03	1500	16	0.000279	0.06219	0.00046	0.05789	0.00046	526	17
02/04	1500	16	0.000612	0.06389	0.00035	0.05486	0.00024	407	10
02/05	1450	14	0.000294	0.06379	0.00113	0.06001	0.00035	604	12
	1500	14	0.000076	0.06147	0.00022	0.06032	0.00032	615	12
02/06	1450	14	0.000105	0.06134	0.00027	0.05988	0.00027	600	10
	1500	12	0.000091	0.06153	0.00064	0.06011	0.00013	608	5
02/07	1450	16	0.000053	0.06151	0.00018	0.06084	0.00023	634	8
	1500	16	0.000077	0.06191	0.00025	0.06087	0.00026	635	9
02/08	1500	14	0.000057	0.06101	0.00027	0.06018	0.00036	610	13
02/09	1500	8	0.000216	0.06468	0.00109	0.06156	0.00110	659	38
02/10	1500	14	0.000027	0.13500	0.00097	0.13452	0.00129	2158	17
02/11	1450	16	0.000061	0.06294	0.00115	0.06224	0.00108	683	37
	1500	12	0.000053	0.06271	0.00014	0.06214	0.00044	679	15
02/14	1450	8	0.000025	0.06022	0.00209	0.05986	0.00213	599	77
	1500	12	0.000060	0.06143	0.00010	0.06055	0.00027	623	10
	1550	14	0.000094	0.06141	0.00020	0.06021	0.00025	612	9
02/17	1450	8	0.000152	0.12924	0.00031	0.12723	0.00116	2060	16
	1500	12	0.000051	0.13038	0.00042	0.12969	0.00044	2094	6
02/20	1500	14	0.000028	0.06131	0.00023	0.06089	0.00018	636	6
02/21	1450	6	0.000045	0.05915	0.00125	0.05850	0.00126	549	47
02/22	1500	14	0.000038	0.06262	0.00091	0.06217	0.00100	680	34
02/23	1450	12	0.000131	0.13104	0.00069	0.12908	0.00088	2086	12
	1500	16	0.000035	0.13096	0.00036	0.13053	0.00038	2105	5
02/24	1450	32	0.000192	0.06432	0.00044	0.06153	0.00055	658	19
	1500	16	0.000219	0.06242	0.00064	0.05897	0.00095	566	35
02/27	1450	16	0.000061	0.06290	0.00046	0.06202	0.00043	675	15
	1500	2	0.000110	0.06266	0.00070	0.06094	0.00096	637	34
Sample	RL10								
10/1		68	0.000030			0.09431	0.00023	1515	4.6
10/2		38	0.000056			0.09427	0.00013	1514	2.6
10/3		8	0.000603			0.12751	0.00254	2064	35.1
10/4		68	0.000019			0.09480	0.00025	1524	4.9
10/5		18	0.000087			0.12980	0.00042	2096	5.7
10/6		22	0.00002			0.09462	0.00021	1521	4.3
10/7		32	0.000096			0.09514	0.00113	1531	22.3
10/8		46	0.000102			0.13909	0.00086	2216	10.6
10/9		16	0.000228			0.18647	0.00378	2712	33.5
10/10		10	0.000095			0.09457	0.00081	1520	16.2
10/11		8	0			0.09572	0.00044	1543	8.7
10/12		40	0.000065			0.09493	0.00044	1527	8.8

Table 4. Whole rock Sm-Nd data for metasedimentary rocks of the Piriá Formation.

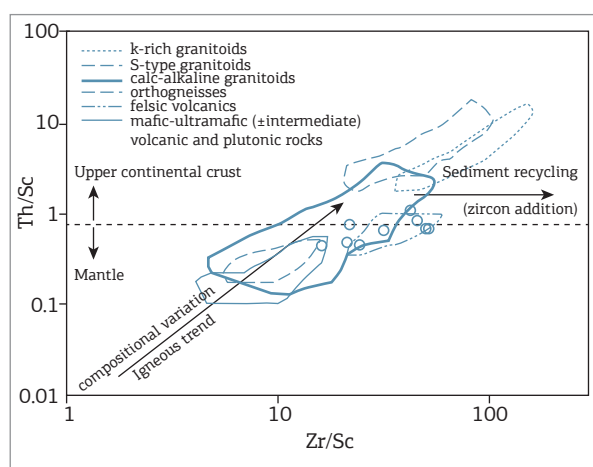
Sample	Rock type	Sm (ppm)	Nd (ppm)	Sm/Nd	f(Sm/Nd)	$^{147}\text{Sm}/^{144}\text{Nd}$	$^{143}\text{Nd}/^{144}\text{Nd}$	eNd(0)	eNd(540)	T_{DM} (Ga)
EK31	subarkose	0.630	3.230	0.1950	-0.395	0.11894	0.511762	-17.09	-11.7	2.06
EL40	arkose	5.955	29.753	0.1988	-0.385	0.12100	0.511913	-14.14	-8.9	1.86
EL42A	arkose	6.512	26.134	0.2492	-0.229	0.15060	0.512064	-11.20	-8.1	2.42
EL37A	greywacke	4.680	27.930	0.1680	-0.480	0.10235	0.511518	-21.85	-15.4	2.09
EL124	sandstone	5.770	29.900	0.1930	-0.407	0.11667	0.512057	-11.33	-5.8	1.55


 Figure 10. Chemical plots for sedimentary rocks of the Piriá Formation, for evaluation of single or multiple sources and hydraulic sorting (see Fralick *et al.* 2009). (A) Zr-Nb, (B) Ce-Th, and (C) V-TiO₂ diagrams.

(Kalsbeek *et al.* 2008), they are also rare and are unlikely sources of the Piriá zircons.

Minor Siderian and Archean ages (2350, 2450 and 2660 Ma) are present in inherited zircon from Rhyacian granitoids of the basement of the Gurupi Belt (Palheta *et al.* 2009, Klein *et al.* 2012) and may additionally suggest an underlying crust of this age. Other subordinate ages (930, 1120, 1290 and 1965 Ma) are also unknown in the region and might have also come from adjacent terranes.

The probability density plots (Fig. 9) of the different samples suggest that the Piriá Basin is a very heterogeneous basin with respect to their sources and paleogeography. Furthermore, differences in the age distribution of different samples suggest that the central (main sector) and eastern sectors might represent isolated segments or even sub-basins. The data of the greywacke sample EL37A (both restricted age range and the presence of crystals with little or no transport abrasion) indicate that their sediments came from a proximal source, probably in a micro-basin with a certain degree of confinement. In addition, the Nd data of this sample, showing T_{DM} of 2.09 Ga, which is slightly


 Figure 11. Zr-Sc versus Th/Sc plot (McLennan *et al.* 1993). The fields of potential Rhyacian source rocks from the Gurupi Belt and São Luís cratonic fragment were drawn with data from Klein *et al.* (2008b, 2009, 2012).

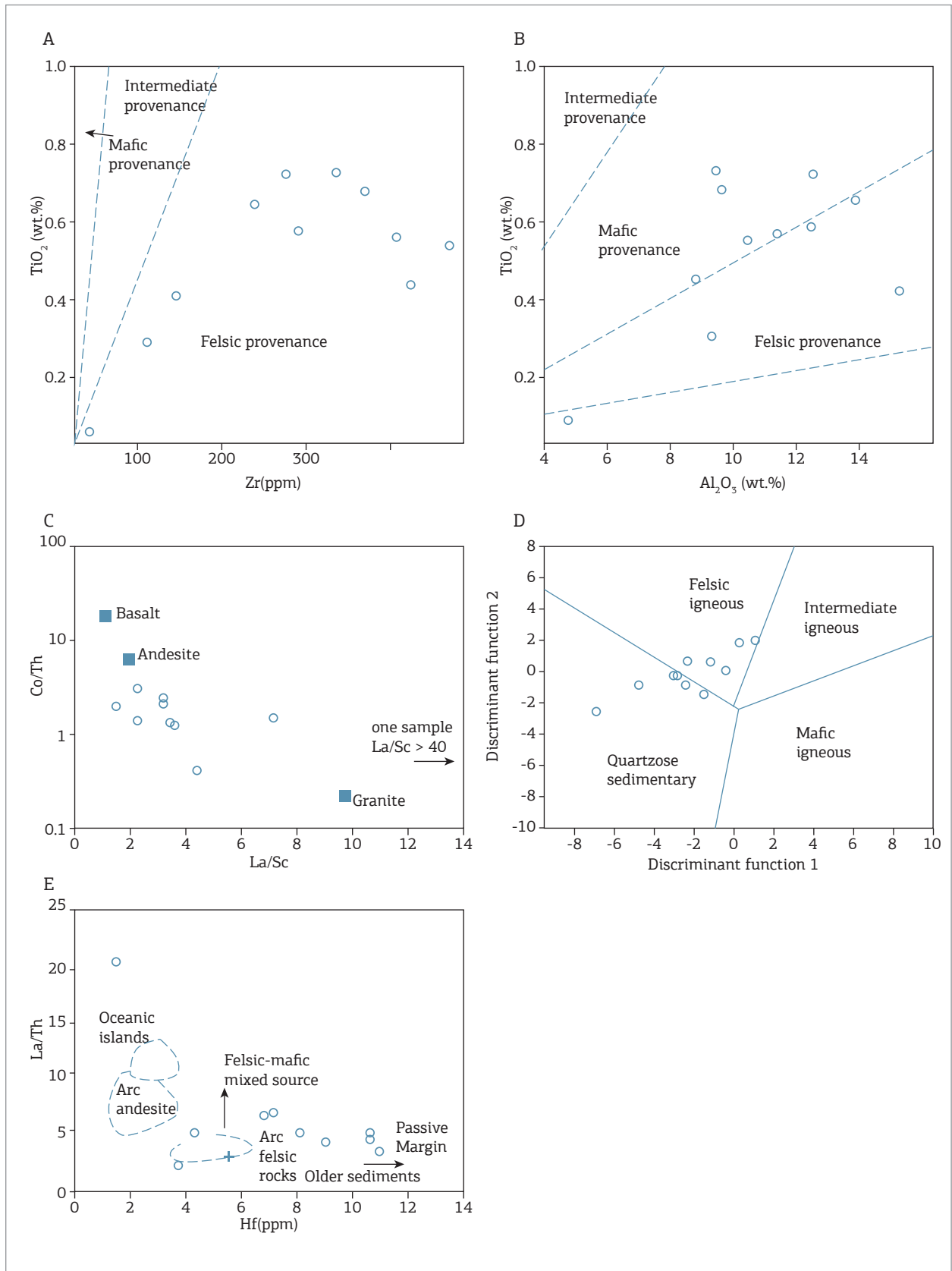


Figure 12. Bivariate plots for provenance evaluation. (A) Zr versus TiO_2 , (B) Al_2O_3 versus TiO_2 , (C) La/Sc versus Co/Th, (D) discriminant function 1 and 2, from Roser & Korsch (1988), (E) Hf versus La/Th (after Floyd & Leveridge 1987); the cross stands for the Upper Continental Crust of Rudnick & Gao (2004).

younger than the younger concordant zircons, indicate that the proximal source is very juvenile and that it possibly contains mafic rocks that do not contribute with zircons to detritus. On the other hand, the major peak of ~ 1500 Ma identified in the sample RL10 suggests that a terrain of this age was the major supplier at this area of the basin, but it had little expression, or is not even identified in other samples. Sample BP02 also highlights the differences in provenance of the central and eastern segment, since it shows the most important age population with ages between 526 and 680 Ma, which is only seen as a minor peak in sample EK31 from the small western segment.

In summary, petrographic, whole-rock geochemistry and Nd data, and detrital zircon geochronology indicate that felsic to intermediate Rhyacian rocks of the São Luís cratonic fragment and Gurupi Belt were the main sources of sediments that filled the central segment of the Piriá Basin. Sedimentary recycling of zircon has also been important, and little Neoproterozoic sediments appear to have contributed with the sedimentary budget in this segment, which is in keeping with the present day knowledge about the evolution of the Gurupi Belt (see Klein *et al.* 2012, Klein & Lopes 2011). However, Neoproterozoic sources were of major importance in the eastern segment. A number of unknown sources are present in the zircon record and deserve further investigation.

Implications for tectonic evolution

The Ediacaran-Cambrian boundary in the South American platform corresponds to the period of closure of the Brasiliano/

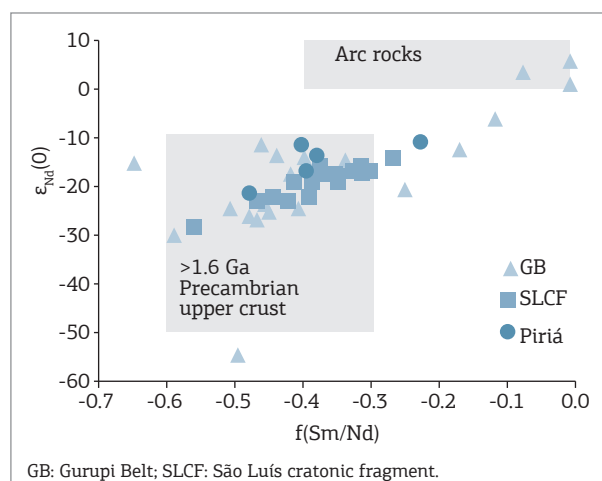


Figure 13. $\epsilon_{Nd}(0)$ versus $f(Sm/Nd)$ diagram for the Piriá Formation in comparison with the composition of potential sources from the São Luís cratonic fragment and Gurupi Belt. Source of data: Klein *et al.* (2005, 2008b, 2009, 2012), Palheta *et al.* (2009), Klein & Lopes (2011). The Precambrian upper crust and arc rocks boxes are from McLennan & Hemming (1992).

Pan-African cycle of orogenies and beginning of the crustal extension and lithosphere thinning (i.e., the transition period, Brito Neves 2002) that gave rise to rifting and formation of intracratonic basins. Basins formed in this period are considered to represent either (1) precursor rifts that underwent slight inversion before the initiation of deposition of the intracratonic basins, such as the Jaibas Basin, which preceded the formation of the Parnaíba Basin (Oliveira & Mohriak 2003), or (2) late- to post-orogenic basins (molasse?) still related to the end of the Brasiliano cycle of orogenies, for instance, the Camaquã Basin in the Sul-Riograndense Shield (Paim *et al.* 2014).

The rocks of the Piriá Formation (Basin) show anquimmetamorphism, which is recorded by the replacement of feldspar clasts by epidote and chlorite, and by the replacement of the pelitic portion of the greywackes matrix by chlorite. In addition, limited deformation is evidenced by minor foliation of the matrix of greywackes, post-sedimentary undulations of sandstone and siltstone strata, and the presence of quartz veins and, locally, epidote-carbonate veinlets. In consequence, we interpret the Piriá Basin as a post-orogenic basin related to the final stages of evolution of the Gurupi Belt.

CONCLUSIONS

Based on rock associations and their field characteristics and relationships, and in whole-rock geochemistry, detrital zircon geochronology and Nd isotopes, the following conclusions can be drawn with respect to the Piriá Basin (Formation):

1. The maximum depositional age is 591 Ma, which places the formation in the Ediacaran-Cambrian boundary.
2. The sedimentary setting comprises fluvial systems, including alluvial fans, plain floods and fluvial canals.
3. Rhyacian felsic to intermediate rocks and recycled sedimentary rocks are the main sources of the sediments that filled especially the main segment of the basin, which likely come from erosion of rock units of the São Luís cratonic fragment and its reworked margin within the Gurupi Belt.
4. Neoproterozoic (526 – 680 Ma) sources were important for the eastern segment of the basin, despite the poverty of known outcropping sources of this age in the region, and it is also recorded as a subordinate source in the western segment.
5. A Mesoproterozoic source of ca. 1500 Ma is well-represented in the conglomerate from the base of the central segment of the Piriá. Rocks of this age are not known so far in the study region.

6. A series of sediment sources with ages that do not match with those found in the São Luís cratonic fragment and Gurupi Belt are also present and their origin remain uncertain. These might represent reworked sedimentary sources, provenance from local sources that were eliminated from the stratigraphic record by erosion or that underlie the exposed terranes, or provenance from sources located outside the study region (Amazonian Craton, Borborema Province?).
7. The basin is associated to the post-orogenic stage of evolution of the Gurupi Belt.

ACKNOWLEDGEMENTS

This work is in part a consequence of projects funded and developed by CPRM – Geological Survey of Brazil in the Gurupi Belt. ELK and CAVM acknowledge the *Conselho Brasileiro de Desenvolvimento Científico e Tecnológico* (CNPq) for research grants (307443/2013-2 and 306856/2010-7, respectively). The reviews of Fabricio Caxito (UFMG) and Feiko Kalsbeek (Geological Survey of Denmark and Greenland) greatly improved the original manuscript.

REFERENCES

- Abreu F.A.M., Villas R.N.N., Hasui Y. 1980. Esboço estratigráfico do Precambriano da região do Gurupi; Estados do Pará e Maranhão. In: Congresso Brasileiro de Geologia, 31, SBG, Camboriú. *Resumos*, v. 2, p. 647-658.
- Almeida F.F.M., Hasui Y., Brito Neves, B.B. 1976. The Upper Precambrian of South America. *Boletim IG-USP*, 7:45-80.
- Almeida F.F.M., Brito Neves B.B.B., Carneiro C.D.R. 2000. The origin and evolution of the South American Platform. *Earth Science Reviews*, 50:77-111.
- Amaral W., Santos T.J., Ancelmi M.F., Fuck R.A., Dantas E.L., Matteini M., Moreto C.P. 2015. 1.57 Ga protolith age of the Neoproterozoic Forquilha eclogites, Borborema Province, NE-Brazil, constrained by U-Pb, Hf and Nd isotopes. *Journal of South American Earth Sciences*, 58:210-222.
- Boynton W.V. 1984. Cosmochemistry of the rare-earth elements: meteorite studies. In: Henderson P. (ed.). *Rare-Earth Elements geochemistry*. Elsevier, Amsterdam, pp. 63-114.
- Brito Neves B.B. 2002. Main stages of the development of the sedimentary basins of South America and their relationship with tectonics of supercontinents. *Gondwana Research*, 5:175-196.
- Bühn B., Pimentel M.M., Matteini M., Dantas E.L. 2009. High spatial resolution analysis of Pb and U isotopes for geochronology by laser ablation multi-collector inductively coupled plasma mass spectrometry (LA-MC-IC-MS). *Anais da Academia Brasileira de Ciências*, 81:1-16.
- Costa J.L., Araújo A.A.F., Villa Boas J.M., Faria C.A.S., Silva Neto C.S., Wanderley V.J.R. 1977. Projeto Gurupi. Belém: DNPM/CPRM, 258 p (inédito).
- Costa J.L. 2000 *Programa Levantamentos Geológicos Básicos do Brasil*. Programa Grande Carajás. Castanhal, Folha SA.23-V-C, Estado do Pará, Belém, CPRM (CD-ROM).
- Cox R., Lowe D.R., Cullers R.L. 1995. The influence of sediment recycling and basement composition on evolution of mudrock geochemistry in the southwestern United States. *Geochimica et Cosmochimica Acta*, 59:2919-2940.
- DePaolo D.J. 1981. A neodymium and strontium isotopic study of the Mesozoic calc-alkaline granitic batholiths of the Sierra Nevada and Peninsular Ranges, California. *Journal of Geophysical Research*, 86:10470-10488.
- Floyd P.A. & Leveridge B.E. 1987. Tectonic environment of the Devonian Gramscatho basin, south Cornwall; framework mode and geochemical evidence from turbidite sandstones. *Journal of the Geological Society*, 144:531-532.
- Fralick P.W., Hollings P., Metsaranta R., Heaman L.M. 2009. Using sediment geochemistry and detrital zircon geochronology to categorize eroded igneous units: An example from the Mesoarchean Birch-Uchi Greenstone Belt, Superior Province. *Precambrian Research*, 168:106-122.
- Ganade de Araújo C.E., Cordani U.G., Basei M.A.S., Castro N.A., Sato K., Sproesser W.M. 2012. U-Pb detrital zircon provenance of metasedimentary rocks from the Ceará Central and Médio Coreau Domains, Borborema Province, NE-Brazil: Tectonic implications for a long-lived Neoproterozoic active continental margin. *Precambrian Research*, 206-207:36-51.
- Gioia S.M.L.C. & Pimentel M.M. 2000. The Sm-Nd method in the geochronology laboratory of the University of Brasília. *Anais da Academia Brasileira de Ciências*, 72:219-245.
- Herron M.M. 1988. Geochemical classification of terrigenous sands and shales from core or log data. *Journal of Sedimentary Petrology*, 58:820-829.
- Kalsbeek F., Frei D., Affaton P. 2008. Constraints on provenance, stratigraphic correlation and structural context of the Volta basin, Ghana, from detrital zircon geochronology: An Amazonian connection? *Sedimentary Geology*, 212:86-95.
- Klein E.L. & Lopes E.C.S. 2011. *Geologia e recursos minerais da Folha Centro Novo do Maranhão – SA.23-Y-D-I, Estados do Maranhão e Pará, Escala 1:1.000.000*. Belém, CPRM – Serviço Geológico do Brasil, CD-ROM.
- Klein E.L. & Sousa C.S.S. 2012. *Geologia e recursos minerais do Estado do Maranhão: texto explicativo. Escala 1:750.000*. Sistema de Informações Geográficas – SIG; Programa Geologia do Brasil – PGB. Belém, CPRM – Serviço Geológico do Brasil, 150 p.
- Klein E.L., Moura C.A.V., Krymsky R., Griffin W.L. 2005. The Gurupi belt in northern Brazil: lithostratigraphy, geochronology, and geodynamic evolution. *Precambrian Research*, 141:83-105.
- Klein E.L., Larizzatti J.H., Luzardo R., Marinho P.A.C., Rosa-Costa L.T., Faraco M.T.L. 2008a. *Geologia e recursos minerais da Folha Cândido Mendes, Estado do Maranhão, Escala 1:100.000*. Belém, CPRM – Serviço Geológico do Brasil, 146 p.
- Klein E.L., Luzardo R., Moura C.A.V., Armstrong R. 2008b. Geochemistry and zircon geochronology of paleoproterozoic granitoids: further evidence on the magmatic and crustal evolution of the São Luís cratonic fragment, Brazil. *Precambrian Research*, 165:221-242.
- Klein E.L., Luzardo R., Moura C.A.V., Lobato D.C., Brito R.S.C., Armstrong R. 2009. Geochronology, Nd isotopes and reconnaissance geochemistry of volcanic and metavolcanic rocks of the São Luís Craton, northern Brazil: implications for tectonic setting and crustal evolution. *Journal of South American Earth Sciences*, 27:129-145.

- Klein E.L., Rodrigues J.B., Lopes E.C.S., Soledade G.L. 2012. Diversity of Rhyacian granitoids in the basement of the Neoproterozoic-Early Cambrian Gurupi Belt, northern Brazil: geochemistry, U-Pb zircon geochronology, and Nd isotope constraints on the Paleoproterozoic magmatic and crustal evolution. *Precambrian Research*, **220-221**:192-216.
- Klein E.L., Tassinari C.C.G., Vaconcelos P.M. 2014. U-Pb SHRIMP and $^{40}\text{Ar}/^{39}\text{Ar}$ constraints on the timing of mineralization in the Paleoproterozoic Caxias orogenic gold deposit, São Luis cratonic fragment, Brazil. *Brazilian Journal of Geology*, **44**:277-288.
- Knudsen C., Thomsen T.B., Kalsbeek F., Kristensen J.A., Vital H., McLimans R.K. 2015. Composition of ilmenite and provenance of zircon in northern Brazil. *Geological Survey of Denmark and Greenland Bulletin*, **33**:81-84.
- Kober B. 1986. Whole grain evaporation for $^{207}\text{Pb}/^{206}\text{Pb}$ age investigations on single zircons using a double filament source. *Contributions to Mineralogy and Petrology*, **93**:482-490.
- LaMaskin T.A., Dorsey R.J., Vervoort J.D. 2008. Tectonic controls on mudrock geochemistry, Mesozoic rocks of eastern Oregon and Western Idaho, U.S.A.: implications for cordilleran tectonics. *Journal of Sedimentary Research*, **78**:765-785.
- Lopes E.C.S. & Klein E.L. 2014. *Folha Santa Luzia do Pará, SA.23-V-C-VI*. Estado do Pará. Programa Geologia do Brasil – PGB, Carta Geológica. Belém: CPRM, escala 1:100.000.
- Ludwig K.R. 2003. User's manual for Isoplot/Ex version 3.00 – A geochronology toolkit for Microsoft Excel. *Berkeley Geochronological Center Special Publication*, n. 4, 70 p.
- McLennan S.M. & Hemming S. 1992. Samarium/neodymium elemental and isotopic systematics in sedimentary rocks. *Geochimica et Cosmochimica Acta*, **56**:887-898.
- McLennan S.M., Hemming S., McDaniel D.K., Hanson G.N. 1993. Geochemical approaches to sedimentation, provenance, and tectonics. In: Johnsson M.J., Basu A. (eds.). Processes controlling the composition of clastic sediments. *Geological Society of America Special Paper*, **284**:21-40.
- Nesbitt H.W. 2003. Petrogenesis of siliciclastic sediments and sedimentary rocks. In: Lentz D.R. (ed.). Geochemistry of sediments and sedimentary rocks: evolutionary considerations to mineral deposit-forming environments. *Geological Association of Canada, GeoText*, vol. 4, pp. 39e51.
- Nesbitt H.W. & Young G.M. 1982. Early Proterozoic climates and plate motions inferred from major element chemistry of lutites. *Nature*, **229**:715-717.
- Oliveira D.C. & Mohriak W.U. 2003. Jaibas Through: an important element in the early tectonic evolution of the Parnaíba interior sag Basin, Northeastern Brazil. *Marine and Petroleum Geology*, **20**:351-383.
- Paim P.S.G., Chemale F.C., Wildner W. 2014. Estágios evolutivos da Bacia do Camaquã (RS). *Ciência e Natura, Santa Maria*, **36**:183-193.
- Palheta E.S., Abreu F.A.M., Moura C.A.V. 2009. Granitóides proterozoicos como marcadores da evolução geotectônica da região nordeste do Pará - Brasil. *Revista Brasileira de Geociências*, **39**:647-657.
- Pastana J.M.N. (Org.). *Turiaçu, folha SA.23-V-DPinheiro, folha SA.23-Y-B: estados do Pará e Maranhão*. Brasília: CPRM, 1995. 205 p. il. + 4 mapas. Escala 1:250.000. Programa Levantamentos Geológicos Básicos do Brasil - PLGB.
- Pettijohn F.J. 1975. *Sedimentary Rocks*. Harper and Row, New York.
- Pinheiro B.L.S., Moura C.A.V., Klein E.L. 2003. Estudo de proveniência em arenitos das formações Igarapé de Areia e Viseu, nordeste do Pará, com base em datação de monocristais de zircão por evaporação de chumbo. Simpósio de Geologia da Amazônia, 8, *Resumos expandidos*, SBG, CD-ROM.
- Potter P.E., Maynard J.B., Depetris P.J. 2005. *Mud and Mudstones: Introduction and Overview*. Heidelberg, Springer-Verlag, 297 p.
- Prosser S. 1993. Rift-related linked depositional systems and their seismic expression. *Geological Society, London, Special Publications*, **71**:35-66.
- Roser B.P. & Korsch R.J. 1988. Provenance signatures of sandstone mudstone suites determined using discriminant function analysis of major-element data. *Chemical Geology*, **67**:119-139.
- Rudnick R. & Gao S. 2004. The composition of the continental crust. In: Rudnick R. (ed.). *Treatise on Geochemistry: The Crust*. Elsevier, Amsterdam, pp. 1-64.
- Rudnick R.L. & Gao S. 2005. Composition of the continental crust. In: Holland H.D. & Turekian K.K. (eds.). *The Crust 3. Treatise on Geochemistry*. Elsevier-Pergamon, Oxford, England, p. 1-64.
- Stacey J.S. & Kramers J.D. 1975. Approximation of terrestrial lead isotope evolution by a two-stage model. *Earth Planetary Science Letters*, **26**:207-221.
- Sun S.S. & McDonough W.F. 1989. Chemical and isotopic systematics of oceanic basalts: implications for mantle compositions and processes. In: Saunders A.D., Norry M.J. (eds.). *Magmatism in ocean basins. Geological Society of London Special Publications*, **42**:313-345.
- Taylor S.R. & McLennan S.M. 1985. *The Continental Crust: Its Composition and Evolution*. Blackwell Scientific Publications, Oxford, UK, pp. 312.
- Truckenbrodt W., Nascimento M.S., Góes A.M. 2003. Minerais pesados em arenitos de formações fanerozoicas no nordeste do Pará e noroeste do Maranhão. In: Horbe A.M.C. & Souza V.S. (eds) *Contribuições à Geologia da Amazônia*, **4**:181-190.
- Villas R.N.N. & Sousa F.D.S. 2007. O granito de duas micas Ney Peixoto, nordeste do Pará: aspectos petrológicos e significado tectônico. *Revista Brasileira de Geociências*, **37**:3-16.